RESEARCH ARTICLE

Open Access

Microglial ferroptotic stress causes non-cell autonomous neuronal death

Jeffrey R. Liddell[1*†] , James B. W. Hilton[1†] , Kai Kysenius[1†] , Jessica L. Billings[1], Sara Nikseresht[1], Lachlan E. McInnes[2], Dominic J. Hare[3], Bence Paul[4], Stephen W. Mercer[1], Abdel A. Belaidi[5], Scott Ayton[5], Blaine R. Roberts[6], Joseph S. Beckman[7], Catriona A. McLean[8], Anthony R. White[9], Paul S. Donnelly[2], Ashley I. Bush[5] and Peter J. Crouch[1*]

Abstract

Background Ferroptosis is a form of regulated cell death characterised by lipid peroxidation as the terminal end-point and a requirement for iron. Although it protects against cancer and infection, ferroptosis is also implicated in causing neuronal death in degenerative diseases of the central nervous system (CNS). The precise role for ferroptosis in causing neuronal death is yet to be fully resolved.

Methods To elucidate the role of ferroptosis in neuronal death we utilised co-culture and conditioned medium transfer experiments involving microglia, astrocytes and neurones. We ratified clinical significance of our cell culture findings via assessment of human CNS tissue from cases of the fatal, paralysing neurodegenerative condition of amyotrophic lateral sclerosis (ALS). We utilised the SOD1[G37R] mouse model of ALS and a CNS-permeant ferroptosis inhibitor to verify pharmacological significance in vivo.

Results We found that sublethal ferroptotic stress selectively affecting microglia triggers an inflammatory cascade that results in non-cell autonomous neuronal death. Central to this cascade is the conversion of astrocytes to a neurotoxic state. We show that spinal cord tissue from human cases of ALS exhibits a signature of ferroptosis that encompasses atomic, molecular and biochemical features. Further, we show the molecular correlation between ferroptosis and neurotoxic astrocytes evident in human ALS-affected spinal cord is recapitulated in the SOD1[G37R] mouse model where treatment with a CNS-permeant ferroptosis inhibitor, Cu[II](atsm), ameliorated these markers and was neuroprotective.

Conclusions By showing that microglia responding to sublethal ferroptotic stress culminates in non-cell autonomous neuronal death, our results implicate microglial ferroptotic stress as a rectifiable cause of neuronal death in neurodegenerative disease. As ferroptosis is currently primarily regarded as an intrinsic cell death phenomenon, these results introduce an entirely new pathophysiological role for ferroptosis in disease.

Keywords Microglia, Ferroptosis, Amyotrophic lateral sclerosis (ALS), Neurotoxic astrocytes, Glial activation, Therapy, Drug discovery, Glia, Neurodegeneration, Iron

[†]Jeffrey R. Liddell, James B. W. Hilton and Kai Kysenius contributed equally to this work.

*Correspondence:
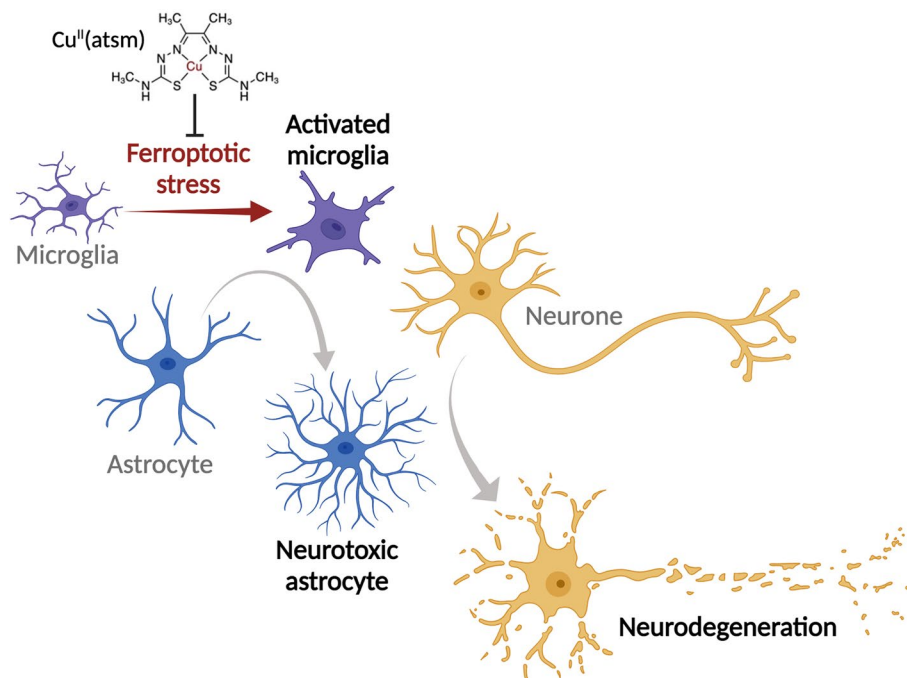Jeffrey R. Liddell
jliddell@unimelb.edu.au
Peter J. Crouch
pjcrouch@unimelb.edu.au
Full list of author information is available at the end of the article

Liddell *et al. Molecular Neurodegeneration* (2024) 19:14

Page 2 of 21

Graphical Abstract

Background

Disease-modifying treatments for neurodegenerative conditions of the central nervous system (CNS) have proved elusive because the major pathways to neuronal death are yet to be elucidated. Defining and targeting histopathologically conspicuous neuronal features has been a focus in the field. However, non-cell autonomous pathways to neuronal death are also implicated, whereby the glial cells that are essential for healthy neuronal function [1, 2] actively contribute to neuronal death in disease [3, 4]. Glial cells, therefore, may represent a more suitable target than neurones for disease-modifying intervention.

The contribution of glial cells to neuronal death is clearly illustrated in amyotrophic lateral sclerosis (ALS), an aggressive adult-onset neurodegenerative disease that results in paralysis and death due to the loss of motor neurones in the brain and spinal cord [5]. Restricting expression of ALS-causing mutations specifically to astrocytes results in neuronal death in vitro [6–8] and in vivo [9], and astrocytes derived from patients with sporadic ALS (i.e. with no known causal mutations) are neurotoxic [10]. Alternatively, diminishing or removing expression of ALS-causing mutations specifically from microglia or astrocytes slows symptom progression [11–15].

In vitro studies show that inflammatory activation of microglia – resident immune cells of the CNS – can provoke naturally neurotrophic astrocytes to convert to a neurotoxic state [16]. This model system indicates an inflammatory signalling pathway in which the interplay between microglia and astrocytes precedes neuronal death. Parallel evidence from ALS, Parkinson's, Alzheimer's, progressive multiple sclerosis and Huntington's disease indicates that microglia and astrocytes conspiring to cause neuronal death may be a common feature of neurodegeneration [16–18].

Here, we examined whether the iron-dependent form of regulated cell death described as ferroptosis [19] contributes to glial-mediated neuronal death. Although ferroptosis can propagate intercellularly [20], it remains regarded as the terminal endpoint for each cell. Results presented herein provide the first evidence for sublethal ferroptotic stress initiating an inflammatory cascade that culminates in non-cell autonomous neuronal death. Furthermore, although ferroptosis is implicated in neurodegenerative disease [21, 22], its pathophysiological role is currently unclear. Our results from human and mouse spinal cord tissue indicate pertinence of glial ferroptotic stress as a cause of neuronal death in neurodegenerative disease.

Liddell *et al. Molecular Neurodegeneration* (2024) 19:14

Page 3 of 21

Methods

Study design

Our examination of ferroptosis contributing to neuronal cell death spanned three areas of investigation: 1. Human disease-affected CNS tissue from cases of ALS; 2. Primary cultures of microglia, astrocytes and neurones; and 3. A transgenic mouse model of ALS. The human tissue analyses provided initial opportunity to verify indications of ferroptosis in neurodegenerative disease then subsequent opportunity to verify disease relevance of findings from the cell culture experiments. The cell culture experiments provided opportunity to examine cell-type specific contributions to neuronal death in vitro with a ferroptotic stress applied as the initiating event. Assessment of the transgenic mouse model of ALS provided opportunity for in vivo verification of in vitro findings and opportunity to assess efficacy of a targeted therapeutic intervention where effects on neuronal survival could be associated with progression of physical symptoms of neurodegeneration.

Human spinal cord tissue

Frozen sections of lumbar spinal cord were obtained from the Victorian Brain Bank (Australia), the MS Society Tissue Bank (UK), MRC London Neurodegenerative Diseases Brain Bank (King's College, London, UK), the University of Maryland Brain and Tissue Bank, a biorepository of the NIH NeuroBioBank (Maryland, USA), and the Sydney Brain Bank. Information on cases used in this study is provided in Supplementary Table 1. Samples were stored at -80 °C until processed for analysis.

Preparation of primary cell cultures

Pregnant C57BL/6JArc females obtained from the Australian Animal Resource Centre were used for generating the neonates used for primary glial cultures and the E14-E15 embryos used for primary neuronal cultures.

Primary mixed glial culture

Mixed glial cultures were prepared according to the method of Hamprecht and Loeffler [23] as previously described [24]. Newborn pups were decapitated then their brains removed and placed in preparation buffer (137 mM NaCl, 5.35 mM KCl, 0.22 mM KH_2PO_4, 0.17 mM Na_2HPO_4, 58.5 mM sucrose, 5.55 mM glucose, 200 U/mL penicillin, and 200 μg/mL streptomycin). Brains were sequentially passed through 250 μm and 135 μm nylon gauze, then centrifuged at 500 RCF for 5 min. Dissociated cells were resuspended in DMEM containing 10% foetal bovine serum, 20 U/mL penicillin and 20 μg/mL streptomycin, and plated at 150,000 cells/cm^2.

Cells were maintained at 37 °C in 10% CO_2 for at least 2 weeks, and media was renewed every 7 days.

Primary microglia culture

Microglia were harvested from mixed glial cultures according to the method of Saura et al. [25], as previously described [24]. Briefly, mixed glial cultures were washed in Dulbecco's modified Eagle's medium (DMEM) before incubation in a 5:1 mix of DMEM and trypsin-EDTA (Sigma #T4174). After detachment of astrocytes, adherent microglia were either washed in DMEM before medium replaced with mixed glial conditioned medium, or scraped, collected, and re-plated in mixed glial-conditioned media at 20,000 cells/cm^2. For the later, medium was changed 7–12 h later to Iscove modified Dulbecco media (IMDM) supplemented with 10% FBS and penicillin/streptomycin. Microglial cultures were maintained at 37 °C in 5% CO_2 for 2 days before experiments.

Primary neurone culture

Neurones were harvested from the cortices of mouse embryos at E14-E15 based on procedures previously described [26], plated at 250,000 cells/cm^2 and maintained in neurobasal medium supplemented with 2% B27, 1 mM glutamine, and 0.1% gentamycin at 37 °C in 5% CO_2 for 6 days before experiments. Cytosine arabinoside (2 μM) was added after 1–2 days in culture. For (1*S*,3*R*)-methyl-2-(2-chloroacetyl)-2,3,4,9-tetrahydro-1-[4-(methoxycarbonyl)phenyl]-1*H*-pyrido[3,4-b]indole-3-carboxylic acid (RSL3) challenge experiments, neurones were maintained in medium supplemented with B27 without antioxidants for 6 days and treated in neurobasal medium conditioned by mixed glial cultures for 2 days. Where indicated, mixed cultures of neurones and astrocytes were generated by omitting cytosine arabinoside.

Primary astrocyte culture

In preliminary RSL3 titration experiments using mixed glial cultures, microglia were almost completely killed at certain concentrations of RSL3 whereas the astrocyte monolayer appeared to be unaffected. After further investigation, we standardised the following conditions to generate astrocyte cultures with microglia removed. Mixed glial cultures were treated with 300 nM RSL3 overnight, followed by washing and 2 days recovery incubation in serum-containing media, before subsequent treatments as indicated. Effectiveness of microglial removal was confirmed by expression of the microglial molecular markers *Cx3cr1* and *C1qa* by quantitative reverse transcription polymerase chain reaction (RT-PCR), and live-cell imaging. From the latter, the total number of cells per field

Liddell *et al. Molecular Neurodegeneration* (2024) 19:14

Page 4 of 21

of view was determined by counting Hoescht-positive nuclei, averaged from 9 fields per condition. The proportion of cells represented by microglia was derived from the morphology of nuclei, isolectin staining and cell mobility. RSL3 toxicity in normal mixed glial cultures was compared to astrocyte cultures with microglia removed (assessed by 3-(4,5-dimethylthiazol-2-yl)-2,5-diphenyltetrazolium bromide (MTT) and lactate dehydrogenase (LDH) assays after 24 h RSL3 treatment) to confirm that exposure to 300 nM RSL3 did not induce a persistent change in the subsequent sensitivity of astrocytes to RSL3 toxicity.

Cell culture experimental treatments
Ferroptosis inducers and inhibitors
For all treatments with ferroptosis inducers and inhibitors, cells were treated for 24 h unless otherwise indicated. Unless otherwise indicated, ferroptosis inducers and inhibitors were applied at the following concentrations: erastin, 10 µM; buthionine sulphoxamine (BSO), 1 mM; ferric ammonium citrate (FAC) as an iron source, 100 µM; liproxstatin-1 (Lip1), 100 nM; ferrostatin-1, 100 nM; deferiprone (DFN), 100 µM.

For viability and lipid peroxidation studies, unless otherwise indicated, RSL3 was applied at 2 µM, Cu^{II}(atsm) was applied at 1 µM, and cells were pre-treated with BSO or erastin for 24 h before additional treatments. Where microglial cultures were treated with RSL3, viability and lipid peroxidation were assessed in presence or absence of Lip1 (20 nM) or DFN (200 µM). For live cell imaging, mixed glial cultures were treated with 100 nM RSL3 unless otherwise indicated, and 2 µM Cu^{II}(atsm).

Where microglia in mixed glial cultures were assessed in response to BSO, cells were treated with BSO for 4 days. Cells also treated with Lip1 in these experiments were co-treated with BSO and Lip1 followed by a second bolus application of Lip1 after 2 days. A single co-treatment of Lip1 was not effective (data not shown). Treating mixed glial cells with BSO for 24 h did not substantially influence microglia cell numbers (data not shown).

For transcript analyses in response to ferroptosis inducers, microglial cultures were treated for 8 h with RSL3 (25 nM) in presence or absence of Lip1 (20 nM) or Cu^{II}(atsm) (200 nM). Mixed glial and astrocyte cultures were treated with either RSL3 (up to 400 nM) or erastin plus iron as FAC (10 µM) in the presence or absence of Lip1, DFN or Cu^{II}(atsm) (500 nM). When RSL3 was applied in combination with iron, transferrin-bound iron was used (10 µM transferrin, 20 µM iron). Addition of transferrin-bound iron to RSL3 treatments was confirmed to exacerbate RSL3 toxicity and increase lipid peroxidation (data not shown).

Glial conditioned media neurotoxicity experiments
Mixed glial, astrocyte and microglial cultures were treated with RSL3 (mixed glial and astrocyte cultures, 100 nM; microglial cultures, 1 nM), erastin, or lipopolysaccharide (LPS; 1 ng/mL), in presence or absence of Lip1 (200 nM) or Cu^{II}(atsm) (200 nM) for 24 h in neurobasal medium (conditioned for 2 days by mixed glial cultures for microglial cultures) before the conditioned media was collected. Protease inhibitor (Roche Complete EDTA-free) was added and the media centrifuged (1000 RCF, 5 min) to remove any cells or debris. The glial-conditioned media was concentrated using pre-wetted 30 kDa molecular weight cut off Amicon Ultra-15 centrifugal filters (4000 RCF, 10 min). To interrogate the impact of the unsequestered small molecular weight species still present in the retentate, the glial-conditioned media was concentrated 20-fold, then retentate was diluted until equivalent to 4-fold concentration of neat media with either filtrate (thus maintaining the original concentration of small molecular weight species), or fresh neurobasal medium (thus diluting small molecular weight species by 5-fold compared to neat media). The latter did not alter results (data not shown). Thus, for consistency, glial-conditioned media in subsequent experiments was concentrated 20-fold, and retentate diluted with filtrate until equivalent to 4-fold concentration of neat media.

Neurones were treated for 24 h with the glial-conditioned media neat or as 4-fold concentrated retentate. When the conditioned media was concentrated more than 4-fold, control retentate (mixed glia treated in the absence of stressors) became neurotoxic (data not shown). Neat conditioned media from RSL3 or erastin-treated glial cells induced mild neurotoxicity (data not shown). Neurones were also treated with conditioned media filtrate to confirm lack of toxicity of unsequestered small molecules including the ferroptosis inducers present in conditioned media. The same concentration of stressors (LPS, RSL3, erastin) was also added directly to control conditioned media and applied to neurones. After treatment, neuronal survival was assessed by MTT assay. The LDH assay could not be used as conditioned media contained a sufficient quantity of LDH activity to interfere with the quantification of neuronal LDH activity.

Preparation of transferrin-bound iron
Transferrin-bound iron was prepared by combining acidic $FeCl_3$ with nitrilotriacetic acid at a 1:10 ratio. This was combined 1:1.4 with 1.4% $NaHCO_3$, and then 1:1 with apo-transferrin at half the molar ratio of $FeCl_3$ in PBS. The final stock solution was 125 µM transferrin, 250 µM iron, 2.5 mM nitrilotriacetic acid, 18 mM HCl, 0.43% $NaHCO_3$, 50% PBS. All experiments with

Liddell *et al. Molecular Neurodegeneration* (2024) 19:14

Page 5 of 21

transferrin-bound iron included an equivalent diluent control, which was prepared as above but with $FeCl_3$ and apo-transferrin omitted. For all analyses, results from cells treated with diluent did not differ from those treated with control media.

Live-cell imaging of lipid peroxidation

Cells were treated with Hoescht-33342 (1 μg/mL) to identify nuclei, Dylight 649-labelled isolectin (Vector labs; 2 μg/mL) to identify microglia, and C11-BODIPY (0.5 μM) for lipid peroxidation for 15 min before addition of treatments and imaging in an Operetta high-content imaging system (PerkinElmer) in a temperature and CO_2-controlled chamber at the indicated time intervals. Fluorescent dyes were imaged as follows: Hoescht-33342 Ex380 ± 40nm/Em410-480nm; isolectin Ex630 ± 20nm/Em640-680nm; reduced C11-BODIPY Ex570 ± 20nm/Em560-630nm; oxidised C11-BODIPY Ex475 ± 30nm/Em500-550nm. Images were captured with Harmony software (PerkinElmer). Image analysis and reconstruction of image sequences into videos was conducted with ImageJ (1.51s) software. To account for potential differences in accumulation of C11-BODIPY, lipid peroxidation was calculated from the ratio of oxidised to reduced C11-BODIPY with background correction. Time-courses of lipid peroxidation were generated from 4–8 imaged fields per condition per biological replicate.

Cell culture C11-BODIPY lipid peroxidation assay

Cells seeded in 96 well culture plates were co-treated with C11-BODIPY (5 μM) and the indicated treatments. After 3 h, cells were washed twice with PBS and fluorescence quantified from the cell monolayer at Ex581nm/Em596nm for reduced C11-BODIPY, and Ex490nm/Em517nm for oxidised C11-BODIPY in an EnSpire multimode plate reader (PerkinElmer). These excitation and emission wavelengths were empirically determined in control experiments. Fluorescence was quantified from 4 points per well, with triplicate wells per treatment. Lipid peroxidation was calculated as the ratio of oxidised to reduced C11-BODIPY after correcting for background fluorescence.

Cell culture viability assays

Cell survival was determined by 3-(4,5-dimethylthiazol-2-yl)-2,5-diphenyltetrazolium bromide (MTT) reduction. Briefly, following treatments, MTT (12 mM) was added to cells to a final concentration of 480 μM. Cells were incubated for 1 h before media was removed and cells lysed in DMSO and absorbance measured at 562nm.

Cell death was determined by lactate dehydrogenase (LDH) activity using a Cytotoxicity Detection Kit (LDH) (Roche). Briefly, following treatments, aliquots of media were sampled and combined with a reaction mix. The change in absorbance was measured over time at 490nm and compared to total LDH activity of control wells treated with 1% triton X-100.

RNA extraction and transcript analyses

All reagents were from Thermo Fisher Scientific unless otherwise indicated and used in accordance with manufacturer's instructions. RNA was isolated from tissue samples or cultured cells using TRI Reagent (Sigma). Contaminating DNA was degraded by treatment of isolated RNA with DNase (Turbo DNA-free Kit). RNA quantity was determined by nanodrop or Qubit RNA HS Assay Kit. cDNA was synthesised using High Capacity cDNA Reverse Transcription Kit.

For human and mouse tissue samples, 25 ng cDNA was pre-amplified for all genes assessed using Taqman PreAmp Master Mix and pooled Taqman Gene Expression Assays. Pre-amplified cDNA was then diluted 20-fold for subsequent analyses. For cell culture samples, 10 ng of cDNA was used per reaction. All samples were run in triplicate per gene.

Quantitative RT-PCR was performed using Taqman Gene Expression Assays and Taqman Fast Advanced Mastermix on a QuantStudio 6 Flex system (Thermo Fisher Scientific). Relative gene expression was determined via the ΔΔ-ct method normalised to *GAPDH* (human tissue), *Gapdh* (mouse tissue) or *Actb* (cell culture) expression. Normalising genes were chosen based on homology/similarity between the resultant gene expression and the corresponding protein expression determined by immunoblotting. Overall transcript signatures represent the average of gene expression z-scores for all genes in a given gene set for each case, animal or culture.

$Cu^{II}(atsm)$ treatment of ALS model mice

Transgenic mice expressing human SOD1 with the G37R mutation [27] were obtained from the Jackson Laboratories (Stock No: 008342) and a colony maintained by breeding $SOD1^{G37R}$ males with C57BL/6JArc females obtained from the Australian Animal Resource Centre. Non-transgenic littermates were used as control animals for all experiments involving $SOD1^{G37R}$ mice.

$SOD1^{G37R}$ mice were treated with $Cu^{II}(atsm)$ commencing when the animals were 140 days old (i.e. after the onset of physical signs of disease). $Cu^{II}(atsm)$ was prepared fresh daily by suspending in standard suspension vehicle (SSV; 0.9% (w/v) NaCl, 0.5% (w/v) Na-carboxymethylcellulose, 0.5% (v/v) benzyl alcohol, 0.4% (v/v) Tween-80) then sonicating. $Cu^{II}(atsm)$ was administered at 30 mg kg^{-1} body weight by gavage twice daily 7 days $week^{-1}$ and continued until the animals were killed for

Liddell *et al. Molecular Neurodegeneration* (2024) 19:14

Page 6 of 21

analysis or until they reached phenotype end-stage. Control groups involved SOD1^{G37R} mice and non-transgenic littermates gavaged with SSV. Treatment groups were balanced for sex of the animals and treatments balanced across litters as best as possible.

The study involved two separate cohorts of animals. The first cohort included animals that were treated and monitored for phenotype progression, continuing until the animals reached phenotype end-stage. The second cohort included animals that were treated as per the first cohort but killed for tissue collection before they reached phenotype end-stage. These animals were killed at 175–195 days old, with all treatment groups balanced for age.

Phenotype assessment of ALS model mice

ALS-like phenotype of the SOD1^{G37R} mice was assessed as previously described [28]. In brief, motor function of the animals was measured using the rotarod assay which involved the accelerating rod paradigm (4–40 rpm for 180 s, performed twice for each day of assessment with only the better performance for each animal used in final data analysis). Survival of the animals was determined as the stage of phenotype progression which necessitated humane killing. Specifically, as soon as the self-righting reflex was lost and persisted for more than 10 s.

Neuronal Gpx4 conditional knockout mice

To examine in vivo responses specifically restricted to cell autonomous neuronal ferroptosis, mice with neuronal knockout of *Gpx4* were generated as previously described [29]. In brief, neuronal inducible *Gpx4* knockout mice (Gpx4NIKO) were generated by two-step cross-breeding between *Gpx4*(f/f) mice (Jackson Laboratories; Stock No: 027964) and the Slick H mice (Jackson Laboratories; Stock No: 012708). To induce *Gpx4* ablation, tamoxifen (T5648, Sigma) was dissolved in corn oil (10 mg/mL) and administered to Gpx4NIKO mice by intraperitoneal injections at 60 mg/kg once per day for 5 consecutive days. *Gpx4*(f/f) mice identically treated with tamoxifen were used as control. For biochemical analysis of mouse tissue, spinal cords were collected 5 days after last tamoxifen injection from mice anaesthetised, perfused and dissected as previously described [30].

Spinal cord tissue processing

For in situ analyses, human spinal cord samples were embedded in Optimal Cutting Temperature compound and cryo-sectioned at 30 μm in the transverse plane, while mouse spinal cord samples were emersion-fixed in 4% paraformaldehyde and embedded in paraffin. For biochemical analyses, human and mouse spinal cord samples were homogenised in tris(hydroxymethyl)-aminomethane-buffered saline (TBS)-based homogenisation

buffer to generate TBS-soluble and -insoluble fractions as previously described [28]. The resultant fractions relatively crudely separate cytosolic components (soluble fraction) from other cellular components such as nuclei and plasma membrane (insoluble fraction). Prior to homogenisation, human spinal cord samples were dissected to collect grey matter-enriched material. Mouse spinal cords were homogenised whole. Assessment of ferroxidase activity involved further processing of the TBS-insoluble fraction, involving supplementation with 1% (v/v) triton X-100 then centrifuging (18,000 RCF, 4 °C, 5 min) to produce triton X-100 soluble extracts. All fractions were assessed for protein content using the Pierce BCA Protein Assay kit, then normalised to a consistent protein concentration by diluting with the appropriate buffers (i.e. TBS-based homogenisation buffer or the TBS-based homogenisation supplemented with triton X-100).

Iron analyses

Iron was quantified in samples using inductively coupled plasma-mass spectrometry (ICP-MS). In situ quantitation of iron in human spinal cords was performed using laser ablation-ICP-MS [31] utilising cryo-sectioned spinal cord as described above. Regions of interest were identified from the resultant in situ quantitative elemental maps. TBS-soluble and -insoluble fractions of spinal cord generated as described above were assessed for iron concentration using 'microdroplet' laser ablation-ICP-MS (LA-ICP-MS) as previously described [32].

Ferroxidase activity assay

Ferroxidase activity in triton X-100 extracts (described above) was determined as previously described [30, 33]. In brief, for each assay run, fresh solutions of 250 μM human apo-transferrin (Sigma) and 1 mM $FeSO_4$ were prepared in N_2-purged dH_2O to mitigate ferroxidase-independent oxidation of iron. Reaction mixtures in HEPES-buffered saline (50 mM HEPES, 150 mM NaCl, pH 7.2) contained 50 μM apo-transferrin and sample (or triton X-100 supplemented TBS-based homogenisation buffer as vehicle control), then reactions initiated by adding $FeSO_4$ to a final concentration of 100 mM. The formation of holo-transferrin was monitored via change in absorbance at 460nm for 5 min at 25 °C.

Glutathione assay

Glutathione was extracted from spinal cord tissue with 1% sulfosalicylic acid based on a previously reported procedure [34]. Aliquots of lysate were combined with a reaction mix to a final concentration of 200 μM NAPDH, 150 μM 5,5'-dithiobis(2-nitrobenzoic acid), 0.1 U glutathione reductase, and 0.5 mM EDTA in 50 mM NaP_i

Liddell *et al. Molecular Neurodegeneration* (2024) 19:14

Page 7 of 21

buffer (pH 7.5). The rate of 5-thio-2-nitrobenzoate generation was followed at 405nm. Tissue glutathione was normalised to tissue wet weight.

Tissue C11-BODIPY lipid peroxidation assay

TBS-insoluble human spinal cord samples were supplemented with 500 nM C11-BODIPY then incubated at ambient temperature for 3 min. Triton X-100 was added to a final concentration of 10% (v/v), samples mixed vigorously, then centrifuged (15,000 RCF, 3 min). Fluorescence in soluble extracts was quantified at Ex581nm/Em596nm for reduced C11-BODIPY, and Ex490nm/Em517nm for oxidised C11-BODIPY in an EnSpire multimode plate reader (PerkinElmer). Lipid peroxidation was calculated as the ratio of oxidised to reduced C11-BODIPY after correcting for background fluorescence. Mouse spinal cord samples were assessed as per human samples except the samples were homogenised in TBS-extraction buffer already supplemented with 500 nM C11-BODIPY.

SDS-PAGE and immunoblotting

Proteins were assessed by western blot following sodium dodecyl sulphate–polyacrylamide gel electrophoresis (SDS-PAGE) resolution using methods previously described [30]. Primary antibodies used were raised to detect: arachidonate 5-lipoxygenase (ALOX5; Sigma, HPA013859); glutathione peroxidase 4 (GPX4; Abcam, ab125066); complement component 3 (C3; Sigma, GW20073F); and GAPDH (Cell Signaling Technology, 2118). Detection utilised horseradish peroxidase conjugated secondary antibodies for anti-rabbit IgG (Cell Signaling Technology, 7074) or anti-chicken IgY (Abcam, ab6877) followed by enhanced chemiluminescence (ECL Advance, GE Healthcare). Abundance of proteins of interest was normalised to the loading control GAPDH and expressed relative to control cases/animals. Full blots are shown in Supplementary Fig. 1.

Immunofluorescent staining

Paraffin embedded mouse spinal cord samples transverse sectioned at 7μm were dewaxed, heat mediated antigen retrieval and blocked with 5% H_2O_2 then goat or donkey serum blocking buffer before immunolabelling as previously described [34]. Primary antibodies were: ALOX5 (Sigma, SAB1410449); lysophosphatidylcholine acyltransferase 3 (LPCAT3; Abcam, ab232958); ionised calcium-binding adapter molecule 1 (IBA1)-Alexa Fluor 647 conjugate (Abcam, ab225261); choline O-acetyltransferase (ChAT; Merck Millipore, AB144P). Secondary antibodies were: goat anti-rabbit IgG Alexa Fluor 488 (Invitrogen, A11008); donkey anti-rabbit IgG Alexa Fluor 647 (Invitrogen, A31573); donkey anti-goat IgG Alexa

Fluor 488 (Invitrogen, A32814). Sections were additionally labelled with 4′,6-diamidino-2-phenylindole (DAPI; Life Technologies, D1306), then coverslipped. Images were captured using a Zeiss Axio Imager M2.

GPX4 activity assay

GPX4 activity in TBS-soluble tissue extracts was determined using phosphatidylcholine hydroperoxide (PC-OOH) as the substrate and RSL3 as a GPX4 selective inhibitor. Procedures used were based on existing protocols [35, 36].

PC-OOH preparation

L-α-Phosphatidylcholine (10 mg) was dissolved in 4 mL 3% (v/v) sodium deoxycholate then diluted to 25 mL using 200 mM borate puffer (pH 9.0). 500,000 U lipoxygenase type I was added, then the solution oxygenised by bubbling through 99% O_2 for 90 min at 37 °C with constant stirring. The PC-OOH solution was then loaded onto a Sep-Pak Vac 35cc C18 cartridge (Waters) which had been activated with 70 mL methanol then pre-equilibrated with 70 mL dH_2O. After loading the sample, the cartridge was washed with a further 70 mL dH_2O. An initial 10 mL methanol was added and the flow-through discarded. An additional 10 mL methanol was then added, and the PC-OOH containing eluent collected. Aliquots were prepared then stored at -30 °C until used.

RSL3 pre-incubations

TBS-soluble tissue extracts containing ~400 μg protein were incubated on ice for 60 min after adding β-mercaptoethanol to a final concentration of 10 mM. Samples were then divided to two equal aliquots. One was supplemented with 16.7 mM RSL3 and the other with an equivalent volume of the RSL3 vehicle solution (DMSO:ethanol at 1:9). These mixtures were incubated at ambient room temperature for 20 min then kept on ice until used in the GPX4 activity assay.

Activity assay

Samples pre-incubated with the GPX4 inhibitor RSL3 or its vehicle control were added to reaction mixture containing 3.3 mM glutathione, 1.1 mM NaN_3, 110 μM NADPH, 330 U glutathione reductase, and 0.22% (v/v) triton X-100. Basal NADPH consumption was monitored at 340nm for 2 min, followed by addition of PC-OOH, then NADPH consumption monitored at 340nm for a further 10–15 min. GPX4 activity was calculated as the rate of RSL3-sensitive, PC-OOH-dependent NADPH consumption min^{-1} mg^{-1} sample protein.

Liddell *et al. Molecular Neurodegeneration* (2024) 19:14

Page 8 of 21

Data analyses

All statistical analyses were performed using GraphPad Prism. Statistical outliers were assessed using the ROUT method [37]. Data are presented as mean ± S.E.M, violin plots (median, ± 25th and 75th percentiles, truncated at min-max values) or z-scores. Significant differences between groups were determined using two-tailed t-tests, one-way ANOVA where multiple comparisons were corrected using Holm-Sidak's test, or Mantel-Cox survival test. Significance was determined as $P < 0.05$.

Results

Markers of ferroptosis are evident in human, sporadic ALS-afflicted tissue

Iron accumulation increases the risk for ferroptosis. Iron elevation in ALS motor cortex is implicated by MRI studies [38–40]. Here, we utilised laser ablation-inductively coupled plasma-mass spectrometry [31, 32] to determine the anatomical distribution of iron in sporadic ALS cases, and found iron accumulation in ALS within the spinal cord grey matter, particularly in the ventral and lateral grey matter regions where motor neurones reside (Fig. 1a, b;

Supplementary Fig. 2a-j), closely corresponding to levels previously reported [41]. The normal tissue partitioning of iron was changed in ALS spinal cord, with accumulation in the tris-buffered saline (TBS)-insoluble fraction of tissue homogenates (Supplementary Fig. 2k-m). These iron changes were accompanied by decreased ferroxidase activity (Fig. 1c), an activity needed for cellular efflux of iron [42, 43], and altered expression of genes associated with iron handling (Fig. 1d, e; Supplementary Fig. 3a), indicating perturbed iron homeostasis in ALS.

By staunching lipid peroxidation, glutathione peroxidase 4 (GPX4) is a major inhibitor of ferroptosis. The inhibition of GPX4 activity is used to model ferroptosis in vitro [44] and its selective ablation from neurones in the murine CNS causes rapid fatality [29]. Our analysis of human spinal cord tissue revealed *GPX4* gene expression, GPX4 protein levels, and GPX4 activity were all unchanged in ALS (Supplementary Fig. 4a-c), as opposed to recent reports of mildly [45] or substantially [46] diminished GPX4 protein in ALS and robust changes we detected in *Gpx4* conditional knockout mice (Supplementary Fig. 4d-f). Nevertheless, the concentration of glutathione, the substrate for GPX4 ferroptosis
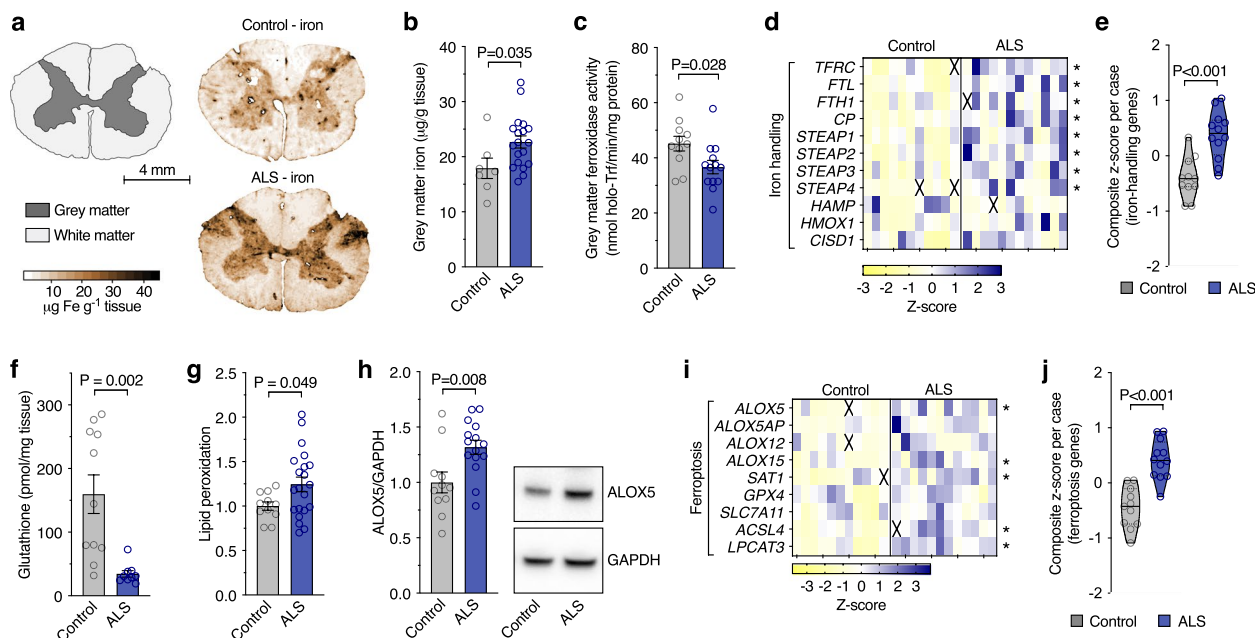

Fig. 1 Markers of ferroptosis in human, ALS-affected spinal cord. **a**, **b** Quantitative in situ mapping of iron in transverse sections of human spinal cord reveals an overall increase in iron in the ALS-affected grey matter. **c** Ferroxidase activity in human, ALS-affected spinal cord. **d**, **e** Transcripts associated with iron handling in human, ALS-affected spinal cord tissue. **f-h** Biochemical markers of ferroptosis (glutathione, lipid peroxidation, and ALOX5 protein levels) in human, ALS-affected spinal cord. **i**, **j** Transcripts associated with ferroptosis in human, ALS-affected spinal cord tissue. Data in **g** and **h** are expressed relative to controls. Data points (**b**, **c**, **e-h**, **j**) represent individual control or ALS cases. Values in transcript heatmaps (**d**, **i**) represent z-scores for individual control and ALS cases. Violin plots in **e**, **j** represent overall transcript signature for features indicated, derived from heatmap data shown in **d**, **i**, respectively. Crosses in heatmaps represent excluded samples. *P* values show significant differences where indicated. Error margins in bar graphs are S.E.M. Solid lines in violin plots represent median, dotted lines represent 25th/75th percentiles, truncated at min-max values

Liddell *et al. Molecular Neurodegeneration*   (2024) 19:14

Page 9 of 21

checkpoint function, was markedly decreased (Fig. 1f), in line with a recent report [47]. This was associated with elevated lipid peroxidation in ALS-affected tissue (Fig. 1g) and also with elevated levels of ALOX5 protein (Fig. 1h), implicated in the initiation of ferroptosis [48]. These findings in tandem with increased aggregated expression of a panel of genes associated with ferroptosis (Fig. 1i; Supplementary Fig. 3b) revealed a molecular signature consistent with ferroptosis in ALS (Fig. 1j).

Microglia have heightened sensitivity to ferroptosis in vitro
As evidence indicates accumulation of iron in ALS spinal cord may be localised to microglia [38], we examined ferroptosis in vitro using a range of inducers and inhibitors (Fig. 2a) to ascertain which cells may be affected. Analysis of primary murine cultures of major cell types in the brain (Supplementary Fig. 5a-c) revealed that microglia were more sensitive to the GPX4 inhibitor RSL3 (LD_{50}

1.77 nM) than astrocytes (LD_{50} 496 nM) and neurones (LD_{50} 82.2 nM, Fig. 2b). Microglia were also distinctly sensitive to the ferroptosis inducers erastin (inhibitor of the glutamate cystine antiporter) and buthionine sulphoximine (inhibitor of γ-glutamylcysteine ligase required for glutathione synthesis; Fig. 2c, d). RSL3 toxicity and lipid peroxidation (detected by the fluorometric lipid peroxidation sensor C11-BODIPY [49]) in microglia were prevented by the ferroptosis inhibitors liproxstatin-1 and deferiprone (Fig. 2e, f). All cultures exhibited similar low cell death in the absence of treatments (Supplementary Fig. 5d).

Comparison of cultured microglia, astrocytes and neurones revealed that the lipoxygenase genes that were prominently elevated in ALS (namely *ALOX5*, *ALOX5AP*, and *ALOX15*; Fig. 1i; Supplementary Fig. 3b) were highly enriched in microglia (Fig. 2g) and increased in response to RSL3 treatment in microglia but not astrocytes, an effect mitigated by liproxstatin-1 (Fig. 2h; Supplementary
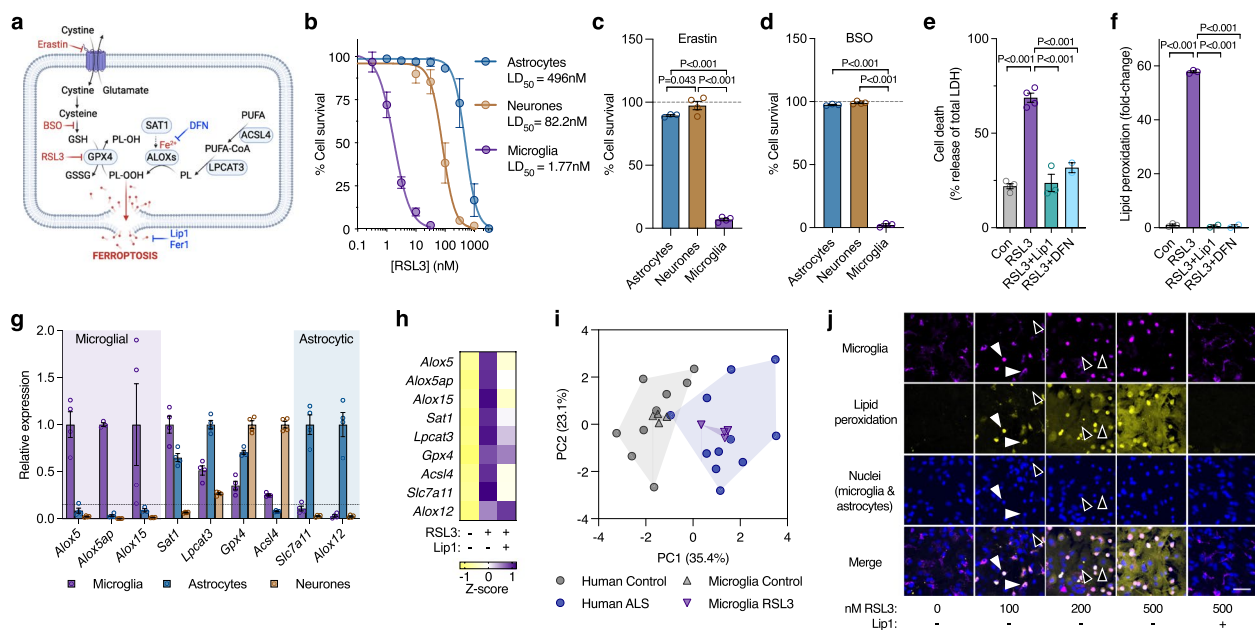

Fig. 2 Microglia have heightened sensitivity to ferroptosis. **a** Ferroptosis is canonically induced by erastin and RSL3, which inhibit the glutamate-cystine antiporter and GPX4, respectively. Ferroptosis is canonically inhibited by lipid radical scavengers liproxstatin-1 (Lip1) and ferrostatin-1 (Fer1). Ferroptosis is also exacerbated by inhibition of glutathione (GSH) synthesis by buthionine sulphoximine (BSO) or by iron (Fe^{2+}), and can be non-specifically inhibited by iron chelators such as deferiprone (DFN). **b-d** Survival (MTT reduction) of cultured microglia, astrocytes and neurones exposed to the ferroptosis inducers RSL3, erastin or BSO ($n=3$–12 for **b**). **e, f** Cytotoxicity (LDH release) and lipid peroxidation in cultured microglia exposed to RSL3 (2 μM) and protection by the inhibitors liproxstatin-1 (Lip1) and deferiprone (DFN). Lipid peroxidation in **f** measured using oxidised:reduced of the ratiometric fluorophore C11-BODIPY. **g** Transcripts associated with ferroptosis in isolated primary murine cultures of microglia, astrocytes and neurones, depicted relative to highest expression. **h** Effect of RSL3 (25 nM; 8 h) on transcripts associated with ferroptosis in cultured microglia, and protection by Lip1 ($n=2$–4). **i** Principal component analysis of ferroptosis genes in response to RSL3 treatment in cultured microglia or ALS in human spinal cord. **j** Lipid peroxidation in response to RSL3 and protection with Lip1 in mixed glial cultures (microglia and astrocytes) detected using oxidised:reduced C11-BODIPY (yellow) showing lipid peroxidation is restricted to microglia (magenta, detected with Dylight 649-labelled isolectin, indicated with white arrowheads) relative to the preponderant astrocytes (black arrowheads). Images derived from Supplementary Video 1. Scale bar (**j**) = 50 μm. *P* values in **c-f** indicate significant differences. Error margins in **b-g** are S.E.M. Data points in **c-g** represent independent cultures. Individual heatmap values in **h** represent mean. Symbols in **i** represent individual control or ALS cases, or independent microglial cultures. Proportion of variance explained by each principal component in **i** is denoted on axes. Data in **i** derived from fold expression change shown in Supplementary Figs. 3b and 5b

Liddell *et al. Molecular Neurodegeneration* (2024) 19:14

Page 10 of 21

Fig. 5e, f). The cell-type expression pattern of ferroptosis genes (Fig. 2g) is closely corroborated by the Brain-RNAseq database [50] (https://www.brainrnaseq.org). Principal component analysis of ferroptosis-related genes revealed RSL3 treatment induced changes in microglia that were similar to those evident in ALS-affected spinal cord (Fig. 2i).

Microglial sensitivity to ferroptosis was further characterised using mixed glial cultures comprised of primary murine microglia and astrocytes. Live cell imaging of mixed glial cultures indicated that lipid peroxidation occurs in microglia at a lower dose of RSL3 than in astrocytes (Fig. 2j; Supplementary Fig. 5g; Supplementary Video 1). Microglia were also more sensitive than astrocytes to other inducers of ferroptosis (erastin, iron, BSO) in mixed glial cultures (Supplementary Fig. 5h-l; Supplementary Videos 2 and 3). Lipid peroxidation was prevented by the ferroptosis inhibitors liproxstatin-1 and deferiprone. Although sufficient to induce microglial lipid peroxidation, neither RSL3 nor erastin plus iron killed microglia under these conditions (Supplementary Fig. 5m, n), providing delineation between ferroptotic stress and ferroptotic cell death.

Ferroptotic stress induces neurotoxic glial activation

Microglial-mediated activation of neurotoxic astrocytes has been demonstrated using the bacterial endotoxin LPS by sequential transfer of conditioned medium from LPS-activated microglia to astrocytes, then from astrocytes onto cultured neurons [16]. Neurotoxicity of conditioned medium from our mixed glial cultures after treating with LPS was consistent with this (Fig. 3a(i)). Moreover, applying RSL3 or erastin to the mixed glia instead of LPS also produced conditioned medium that was neurotoxic (Fig. 3a(i)), demonstrating that these canonical inducers of ferroptosis, when applied to glial cells, produced a comparable neurotoxic result. The absence of neuronal death from equivalent treatments applied directly to the neurons confirmed the role of glial cells in this model of non-cell autonomous neuronal death (Fig. 3a(v)). Moreover, mitigation of neurotoxicity from RSL3 or erastin-induced glial conditioned medium by treating the glial cells with liproxstatin-1 supported the role of glial ferroptotic stress as the initiating event (Fig. 3a(i)).

Conditioned media in all experiments was fractionated using 30 kDa molecular weight cut-off filters (Supplementary Fig. 6a). The concentrated filter retentate increased the neurotoxicity of neat conditioned medium (Supplementary Fig. 6b), indicating a gain of toxicity in the conditioned medium consistent with neurotoxic astrocyte activation, as opposed to a loss of trophic support. The latter is further supported by the use of

sublethal concentrations of RSL3 or erastin excluding glial death as a contributing factor (Supplementary Fig. 5m, n). Furthermore, media retained by the filters was neurotoxic whereas media that passed through was not (Supplementary Fig. 6c). This indicates neurotoxicity was not instigated by free molecules with a molecular mass < 30 kDa.

Greater susceptibility of microglia to ferroptotic stimuli than astrocytes and neurones (Fig. 2b-d, j) raised the possibility that neurotoxicity of the ferroptosis-induced glial conditioned medium was the result of a cascade of events instigated by a microglial response to ferroptotic stress. Although not involving ferroptosis, the LPS-induced, microglial-mediated activation of neurotoxic astrocytes [16] provides a precedent for such an inflammatory signalling pathway to neuronal death involving an interplay between the two glial cell types. Medium from isolated astrocytes or microglia treated with ferroptosis inducers or LPS was not toxic to neurons (Fig. 3a(ii,iii)), whereas microglial conditioned medium was toxic to cultures comprising both neurones and astrocytes (Fig. 3a(iv)). This indicates the neurotoxic cascade was initiated in microglia, but astrocytes were required for neurotoxicity. In contrast to mixed glial cultures, RSL3 at 100 nM and erastin were toxic to isolated microglia (Fig. 2b, c). To exclude the possibility that neurotoxicity was triggered by microglial death, microglia were exposed to a titration of RSL3 (Supplementary Fig. 6d). Medium from microglia treated with subtoxic RSL3 (1 nM) was toxic to cultures containing neurones and astrocytes (Fig. 3a(iv)). This indicates sublethal ferroptotic stress in isolated microglia is sufficient to induce neurotoxic astrocyte activation. Interestingly, medium from microglia treated with 300 nM RSL3 was not neurotoxic, whereas media from microglia treated with erastin or up to 100 nM RSL3 were neurotoxic (Supplementary Fig. 6d). Given that higher doses of RSL3 induce not only more extensive but also more rapid lipid peroxidation (Supplementary Fig. 6e), the former indicates medium containing rapidly killed microglia is not neurotoxic, whereas the latter suggests treatments that eventually kill microglia are sufficient to induce an inflammatory response in microglia before they succumb.

LPS-treated microglia up-regulate *C1qa*, *Il1a* and *Tnf*, provoking astrocytes to adopt a neurotoxic phenotype termed A1 with a gene expression signature distinct from alternatively activated astrocytes, termed A2 [16]. In our cell culture model in which microglia and astrocytes were grown together, both LPS and RSL3 treatments up-regulated microglial *C1qa*, *Il1a* and *Tnf* (Supplementary Fig. 7a). We analysed expression of a

Liddell *et al. Molecular Neurodegeneration* (2024) 19:14

Page 11 of 21

subset of the genes reported for neurotoxic astrocytes [16] and found that RSL3 did not induce a robust A1 phenotype (Supplementary Fig. 7a). However, from those analysed, we identified certain genes whose expression was increased by both RSL3 and LPS (Supplementary Fig. 7b, c), and thus associated with the neurotoxic phenotype. Furthermore, principal component analysis showed that RSL3 (but not LPS) induced changes in these genes that recapitulated changes observed in ALS-affected spinal cord (Supplementary Fig. 7d).

Inducers of ferroptosis applied to mixed glial cultures up-regulated microglial *C1qa*, *Il1a* and *Tnf*, along with the expression of identified genes associated with neurotoxic glia, and these markers were suppressed by the ferroptosis inhibitors liproxstatin-1 and deferiprone (Fig. 3b; Supplementary Fig. 7e). Isolating astrocytes from mixed glial cultures (Supplementary Fig. 8a-g) before treating with ferroptosis inducers abolished the

upregulation of genes associated with neurotoxicity (Fig. 3c; Supplementary Fig. 8h-k), corroborating the conditioned medium findings (Fig. 3a) that the neurotoxic activation of glia by ferroptotic stress requires the presence of microglia.

Markers of neurotoxic glial activation correlate with ferroptosis in ALS

Complement component 3 (C3) is one of the most prominent molecular markers delineating neurotoxic reactive astrocytes from alternatively activated astrocytes, and is reportedly elevated in neurodegenerative disease [16, 51]. Our assessment of C3 protein in human, ALS-afflicted spinal cord corroborates this finding (Fig. 4a). Further, our analysis of gene expression changes indicated signatures for A1 and A2 astrocytes, and the subset of genes we identified to be associated with neurotoxic glia, are all elevated in
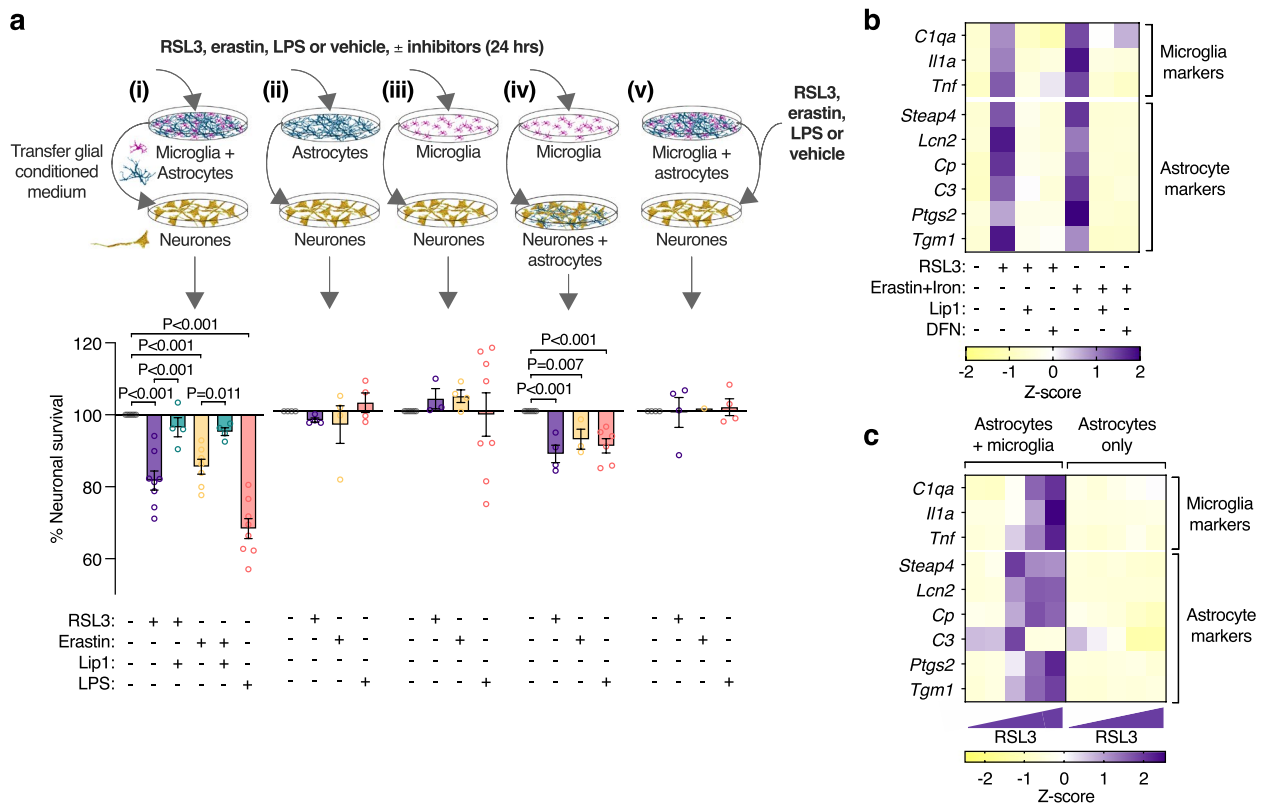

Fig. 3 Ferroptotic stress induces neurotoxic glial activation. **a** Conditioned medium from mixed glial cultures (i) treated with RSL3, erastin or LPS is toxic to cultured neurones (MTT reduction). Toxicity is alleviated by liproxstatin-1 (Lip1). Conditioned medium from identically treated isolated astrocyte (ii) or microglia (iii) cultures is not neurotoxic, whereas conditioned medium from isolated microglia is neurotoxic to neurones cultured with astrocytes (iv). Adding RSL3, erastin or LPS directly onto neurones is not toxic (v). Isolated microglia cultures treated with 1 nM RSL3. All other cultures treated with 100 nM RSL3. Error margins are S.E.M. *P* values indicate significant differences. Procedure for exposing neurones to glial conditioned medium is depicted in Supplementary Fig. 6a. Glial conditioned medium is concentrated using 30 kDa MWCO filters. Data points in **a** represent independent cultures. **b** Effect of RSL3 (200 nM) or erastin plus iron (as ferric ammonium citrate)-induced ferroptotic stress on expression of genes associated with activation of microglia and astrocytes in mixed glial cultures, and protection by Lip1 or deferiprone (DFN). **c** RSL3 (100–400 nM) induced expression of glial activation genes in mixed glial cultures (astrocytes & microglia) but not astrocytes alone. Individual heatmap values (**b**, **c**) represent mean (*n* = 3–6)

Liddell *et al. Molecular Neurodegeneration* (2024) 19:14

Page 12 of 21

ALS-affected spinal cord (Fig. 4b, c; Supplementary Fig. 3c). The expression of genes associated with ferroptosis (Fig. 1i, j) were positively correlated to those associated with neurotoxic glial activation in human, ALS-affected spinal cord (Fig. 4d).

ALS model mice recapitulate signs of ferroptosis and neurotoxic glial activation evident in human ALS-afflicted tissue

To further examine ferroptosis and neurotoxic glial activation, we assessed spinal cord tissue collected from the SOD1[G37R] mouse model of ALS [27]. Analysis of spinal cord tissue collected from animals at the mid-symptom age of 175–195 days revealed accumulation of iron, loss of ferroxidase activity, and altered expression of iron handling genes (Fig. 5a-d; Supplementary Fig. 9a), indicating disrupted iron homeostasis remarkably similar to human ALS-afflicted tissue (Fig. 1a-e). Lipid peroxidation was also increased in the SOD1[G37R] mouse model (Fig. 5e). GPX4 protein was decreased (Fig. 5f) whereas glutathione was unchanged (Supplementary Fig. 9b), in contrast to human ALS tissue where GPX4 was unchanged (Supplementary Fig. 4a-c) and glutathione was decreased (Fig. 1f). A gene expression signature consistent with ferroptosis was also evident in the mouse model (Fig. 5g, h; Supplementary Fig. 9c). These data show that diverse features of ferroptosis evident in human, sporadic cases of ALS are reproduced in this mutant SOD1 model of the disease. Molecular markers of neurotoxic glial activation were also elevated in the SOD1[G37R] mouse model (Fig. 5i, j; Supplementary Fig. 9d), consistent with data reported for the SOD1[G93A] model [51].

Markers of ferroptosis were assessed in the SOD1[G37R] mouse model at the cellular level by immunofluorescence. The microglial protein ALOX5 was elevated in microglia (Fig. 5k, l), in line with *Alox5* transcript expression in the mice (Fig. 5g) and ALOX5 expression at the transcript and protein level in ALS tissue (Fig. 1h, i). LPCAT3, involved in generation of ferroptosis-sensitive lipids (Fig. 2a), and whose expression is not specific to microglia (Fig. 2g), was also elevated in the SOD1[G37R] mouse model, specifically in microglia (Fig. 5m, n), with no change in LPCAT3 in motor neurones nor total LPCAT3 (Supplementary Fig. 10a-c). Using conditional *Gpx4* knockout mice in which deletion of *Gpx4* is restricted to neurones, LPCAT3 was specifically elevated in spinal cord motor neurones (Supplementary Fig. 10d, e). Despite the evident and reported gliosis in the spinal cord of these mice [29], LPCAT3 was unchanged in microglia (Supplementary Fig. 10f, g), verifying that LPCAT3 protein expression is responsive to ferroptosis, that an increase in motor neurone LPCAT3 would be expected in SOD1[G37R] mice if indeed ferroptosis was present in those cells, and that elevated LPCAT3 expression in microglia is not associated with generalised activation of microglia.

Cu[II](atsm) protects against glial ferroptosis and neurotoxic glial activation

The cell and blood–brain barrier permeant small molecule Cu[II](atsm) (Fig. 6a) exhibits anti-ferroptotic activity in monocultures of immortalised cell lines, primary neurones and cell-free assays [52, 53]. In line with this, we found that Cu[II](atsm) exhibits anti-ferroptotic activity in glial cells. We found that Cu[II](atsm) prevented
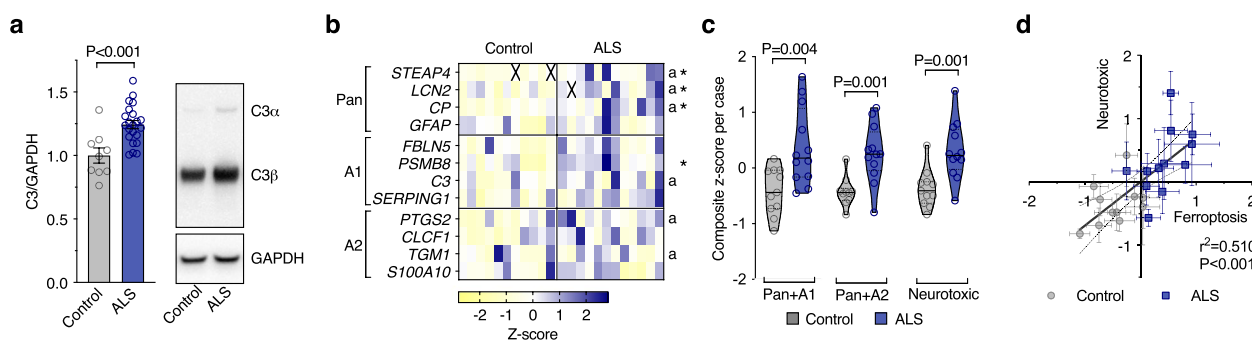

Fig. 4 Markers of glial activation and ferroptosis are correlated in human, ALS affected spinal cord. **a** Protein levels of neurotoxic astrocyte marker C3 expressed relative to controls. **b, c** Transcripts associated with glial activation, highlighting selected markers designated for pan, A1 and A2 activation. Genes associated with neurotoxicity in vitro (shown in Supplementary Fig. 7) are indicated by 'a'. Violin plots in **c** represent overall transcript signature for features indicated, derived from heatmap data shown in **b**, including genes associated with neurotoxicity in vitro (Neurotoxic). **d** Correlation between overall transcript signatures for ferroptosis and glial activation associated with neurotoxicity. Symbols represent composite z-scores for ferroptosis (from Fig. 1j) and glial activation associated with neurotoxicity (from **c**) for corresponding individual cases. *P* values show significant differences where indicated (**a**, **c**) or significance of correlation (**d**). Data points in **a**, **c**, **d** represent individual control or ALS cases. Values in transcript heatmap (**c**) represent z-scores for individual control and ALS cases. Crosses represent excluded samples. Error margins are S.E.M. per mean (**a**) or per case (**d**), or 95% confidence interval of linear regression (dashed lines) in **d**. Solid lines in violin plots represent median, dotted lines represent 25th/75th percentiles, truncated at min-max values
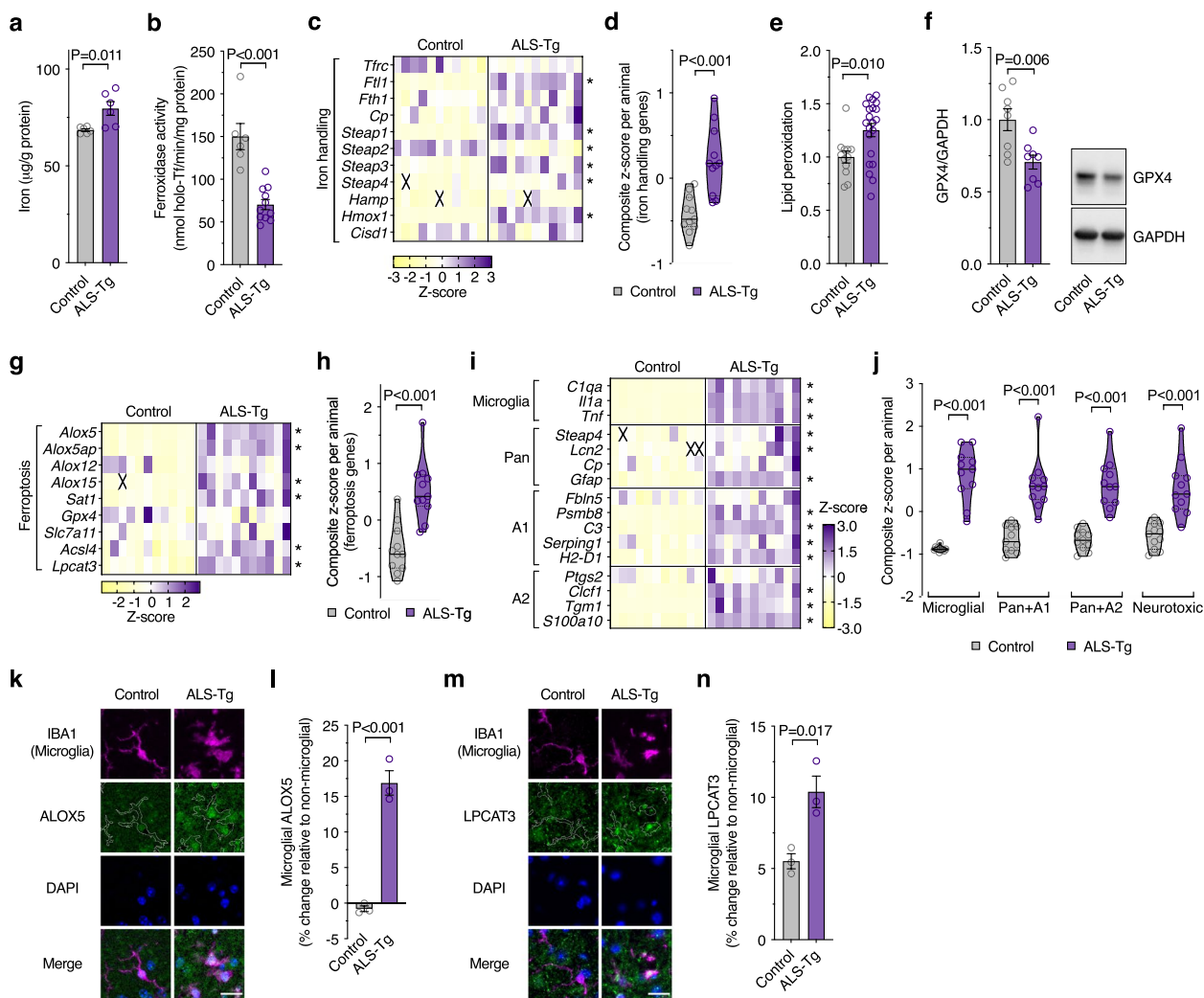
Liddell *et al. Molecular Neurodegeneration* (2024) 19:14

Page 13 of 21

Fig. 5 ALS model mice recapitulate features of ferroptosis and neurotoxic glia evident in human ALS-affected spinal cord. **a**-**d** Markers associated with iron are perturbed in spinal cord of transgenic SOD1^{G37R} ALS model mice (ALS-Tg) compared to non-transgenic littermates (Control), including elevated iron, diminished ferroxidase activity and altered expression of iron handling genes. **e**-**h** Spinal cord tissue from transgenic SOD1^{G37R} ALS model mice display features of ferroptosis, including elevated lipid peroxidation, diminished GPX4 protein level, and altered transcripts for ferroptosis related genes. **i**, **j** Relative expression changes for genes associated with neurotoxic glial activation in spinal cord of SOD1^{G37R} and control mice. Violin plots in **j** represent overall transcript signature for features indicated, derived from heatmap data shown in **i**, including genes associated with neurotoxicity in vitro (Neurotoxic; shown in Supplementary Fig. 7). **k** Representative immunofluorescence for microglial marker IBA1 (magenta), ferroptosis-related protein ALOX5 (green) and nuclear marker DAPI (blue) in spinal cord ventral horn of SOD1^{G37R} and control mice. **l** Microglial ALOX5 quantitated from **k**. **m** Representative immunofluorescence for IBA1 (magenta), ferroptosis-related protein LPCAT3 (green) and DAPI (blue) in spinal cord ventral horn of SOD1^{G37R} and control mice. **n** Microglial LPCAT3 quantitated from **m**. Data in **e** and **f** are expressed relative to controls. *P* values show significant differences where indicated. Data points (**a**, **b**, **d**-**f**, **h**, **j**, **l**, **n**) represent individual SOD1^{G37R} or control animals. Error margins in **a**, **b**, **e**, **f**, **l**, **n** are S.E.M. Values in transcript heatmaps (**c**, **g**, **i**) represent z-scores for individual SOD1^{G37R} or control animals, and crosses represent excluded samples. Violin plots in **d**, **h**, **j** represent overall transcript signature derived from heatmap data shown in **c**, **g**, **i**, respectively, where solid lines represent median, dotted lines represent 25th/75th percentiles, truncated at min-max values. Outline of IBA1-positive microglia are overlaid with ALOX5 and LPCAT3 in **k** and **m**, respectively. Scale bar (**k**, **m**) = 20 μm

RSL3-induced lipid peroxidation and cytotoxicity in mixed glial cultures at concentrations similar to liproxstatin-1 and ferrostatin-1 (Fig. 6b; Supplementary Fig. 11a-b). Cu^{II}(atsm) also prevented the cytotoxicity of other inducers of ferroptosis (BSO, erastin, iron; Supplementary Fig. 11c-d), prevented RSL3-induced lipid peroxidation and cytotoxicity in isolated microglia (Supplementary Fig. 11e-h; Supplementary Video 4), and prevented microglial lipid peroxidation in mixed glial cultures treated with sublethal RSL3 (Supplementary Fig. 11i-j; Supplementary
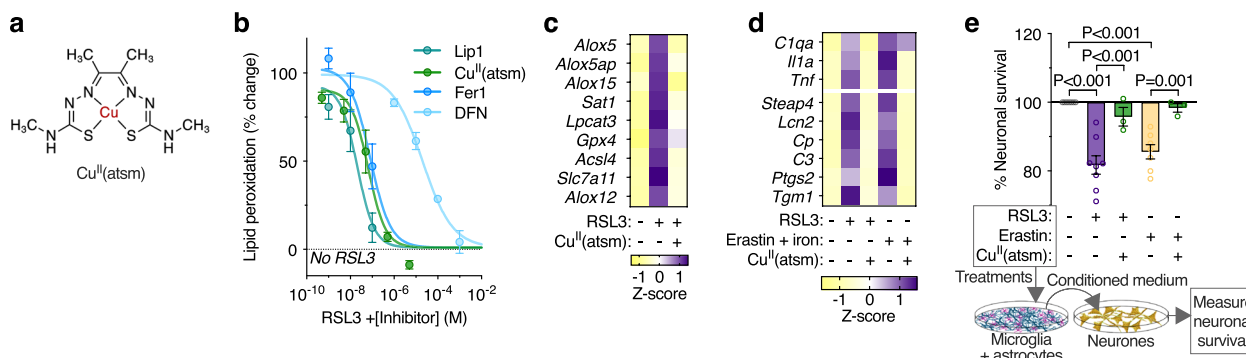
Fig. 6 The metallocomplex Cu^{II}(atsm) protects against glial ferroptosis and neurotoxic glial activation in vitro. **a** Chemical structure of Cu^{II}(atsm). **b** Cu^{II}(atsm) prevents RSL3-induced (2 μM) lipid peroxidation in mixed primary cultures of murine microglia and astrocytes, with efficacy similar to the ferroptosis inhibitors liproxstatin-1 (Lip1) and ferrostatin-1 (Fer1). Lipid peroxidation measured as oxidised:reduced C11-BODIPY ($n = 2$–4). **c** Cu^{II}(atsm) mitigates RSL3-induced (25 nM; 8 h) expression of genes associated with ferroptosis in microglial cultures ($n = 3$–4). **d** Cu^{II}(atsm) mitigates ferroptotic stress-induced expression of genes associated with activation of microglia and astrocytes in mixed glial cultures ($n = 3$–6; RSL3 200 nM; iron as ferric ammonium citrate). **e** Cu^{II}(atsm) inhibits RSL3- (100 nM) and erastin-induced generation of neurotoxic glial conditioned medium, resulting in neuroprotection (MTT reduction). Data points in **e** represent independent cultures. *P* values (**e**) indicate significant differences where indicated. Error margins in **b**, **e** are S.E.M. Symbols (**b**) or individual heatmap values (**c**, **d**) represent mean

Video 5). Furthermore, Cu^{II}(atsm) mitigated RSL3-induced up-regulation of ferroptosis-related genes in isolated microglia (Fig. 6c; Supplementary Fig. 12a), and gene expression associated with neurotoxic glial activation induced by sublethal RSL3 or erastin in mixed glial cultures (Fig. 6d; Supplementary Fig. 12b). Concordantly, Cu^{II}(atsm) suppressed the neurotoxicity of glial conditioned medium induced by RSL3 or erastin (Fig. 6e).

Pharmacological mitigation of markers of ferroptosis and neurotoxic glial activation associates with disease modification in vivo

To further interrogate the relationship between ferroptosis and neurotoxic glial activation, we treated a cohort of SOD1^{G37R} ALS model mice with Cu^{II}(atsm), with treatment commencing after the onset of physical signs of disease (Fig. 7a). Supportive of previous studies [28, 54–58], treatment with Cu^{II}(atsm) slowed the rate of decline in motor function and resulted in an overall improvement in survival (Fig. 7b-d).

Analysis of spinal cord tissue collected from animals at the mid-symptom age of 175–195 days revealed Cu^{II}(atsm) treatment mitigated elevated iron levels, loss of ferroxidase activity, elevated lipid peroxidation and decreased GPX4 protein (Fig. 7e-h), while glutathione levels remained unchanged (Supplementary Fig. 13a). Treatment with Cu^{II}(atsm) also broadly mitigated the increased expression of genes related to ferroptosis and neurotoxic glial activation (Fig. 7i, j; Supplementary Fig. 13b, c), particularly for genes enriched in microglia, consistent with the reported in vitro anti-ferroptosis activity of Cu^{II}(atsm) [52] and as we found in cultured glial cells (Fig. 6).

Interestingly, Cu^{II}(atsm) treatment modestly decreased expression of *Gpx4* below control and increased *Acsl4* and *Lpcat3* (Fig. 7i, j; Supplementary Fig. 13b, c).

Molecular markers of neurotoxic glial activation correlated with the expression signature for ferroptosis in the mice (Fig. 7k), thus reproducing the association between ferroptosis and neurotoxic glial activation observed in human, sporadic ALS-affected spinal cord (Fig. 4d). Consistent with the anti-ferroptotic action of Cu^{II}(atsm) and ferroptosis inducing glial activation in vivo, treatment with Cu^{II}(atsm) proportionately suppressed the molecular signature of both ferroptosis and neurotoxic glial activation in the SOD1^{G37R} mouse model (Fig. 7k).

Congruence across experimental paradigms and human, disease-affected tissue in molecular signatures for ferroptosis and neurotoxic glial activation

Principal component analysis revealed that changes in expression of genes related to ferroptosis or to neurotoxic glial activation were remarkably similar between glial cells treated with RSL3, sporadic ALS-affected tissue, and the SOD1^{G37R} mouse model (Fig. 8a, b). For ferroptosis genes, PC1 accounted for 49.7% of total variance and strongly segregated ALS cases, ALS model mice and RSL3-treated microglia from controls (Fig. 8a). *Lpcat3*, *Acsl4*, *Alox5*, *Alox5ap*, *Alox15* and *Sat1* were highly correlated across all samples (Supplementary Fig. 14a), and accounted for most of the variance in PC1, including almost 80% of the variance for *Lpcat3* (Supplementary Fig. 14c), indicating these genes strongly contribute to the segregation of ALS groups from controls. *Gpx4* and
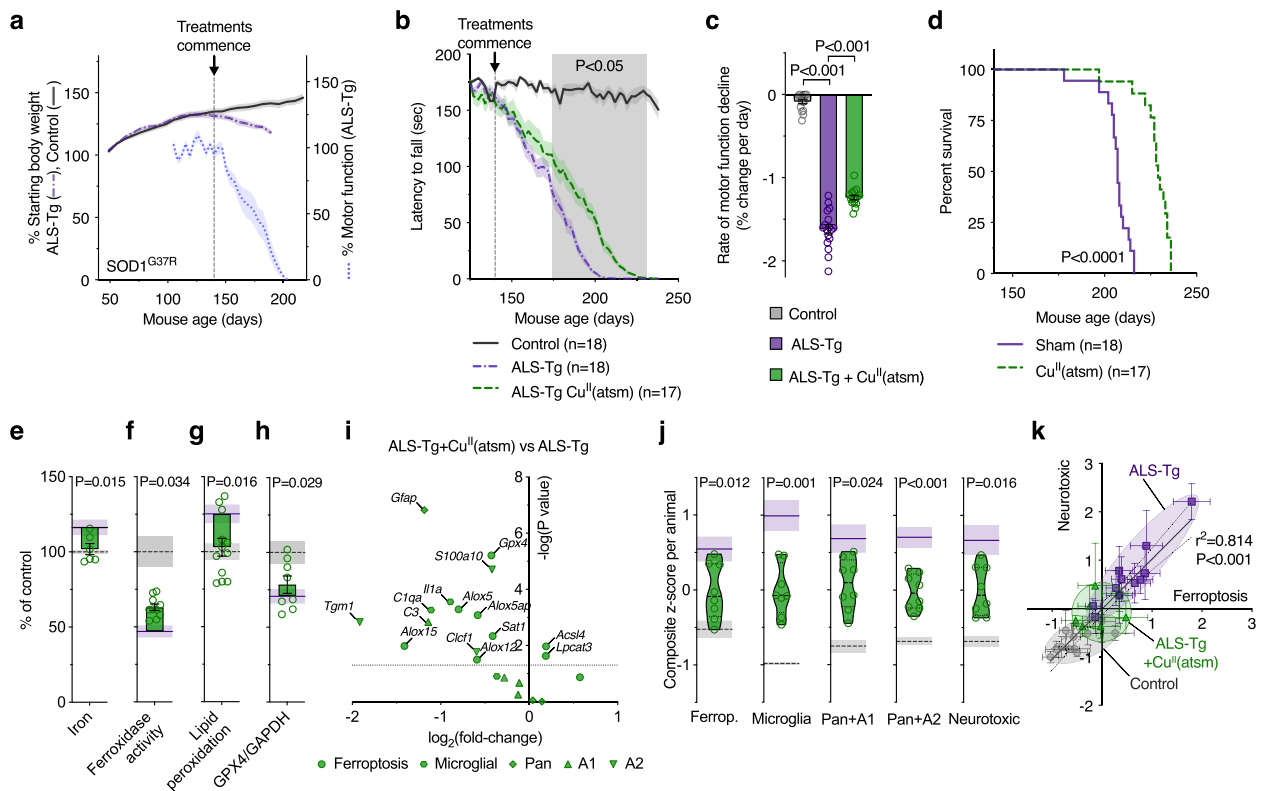
Liddell *et al. Molecular Neurodegeneration* (2024) 19:14

Page 15 of 21

Fig. 7 Treatment with Cu^{II}(atsm) is protective and mitigates markers of ferroptosis and glial activation in ALS model mice. **a** Stage of phenotype progression in transgenic SOD1^{G37R} ALS model mice (ALS-Tg) at which treatment with Cu^{II}(atsm) commenced for the present study. Percentage starting body weight for SOD1^{G37R} mice is expressed relative to body weight per animal at 50 days old. Percentage motor function (rotarod assay) is expressed relative to average performance per animal over the period 125–139 days ($n = 14$–21 animals). **b** Effect of Cu^{II}(atsm) at 30 mg/kg body weight twice daily on motor function of SOD1^{G37R} mice. **c** Rate of motor function decline in SOD1^{G37R} mice derived from data in **b**. **d** Cu^{II}(atsm), administered orally commencing at the post symptom-onset age of 140 days, extends survival of the SOD1^{G37R} mouse model of ALS. **e-h** Therapeutic outcomes for Cu^{II}(atsm) in the SOD1^{G37R} mice are associated with improved biochemical markers of ferroptosis, including decreased iron levels, increased ferroxidase activity, decreased lipid peroxidation and increased GPX4 protein in extracted spinal cord tissue. Lipid peroxidation in **g** measured as oxidised:reduced C11-BODIPY. **i** Volcano plot of transcript analyses for genes associated with ferroptosis and neurotoxic glial activation in SOD1^{G37R} mouse spinal cord tissue treated with Cu^{II}(atsm) compared to SOD1^{G37R} mice without Cu^{II}(atsm) treatment. **j** Overall transcript signature for ferroptosis and neurotoxic glial genes are mitigated by Cu^{II}(atsm) treatment, including genes associated with neurotoxicity in vitro (Neurotoxic), derived from **i** and Fig. 5g-j. **k** Correlation between overall transcript signatures for ferroptosis and neurotoxic glia (from **j** and Fig. 5h, j). Symbols represent individual animals. In **e-h**, **j**, data points represent individual SOD1^{G37R} mice treated with Cu^{II}(atsm); purple solid lines and grey dashed lines and represent mean of SOD1^{G37R} without Cu^{II}(atsm) treatment and control non-transgenic littermates, respectively. Error margins are S.E.M. in line plots (**a**, **b**), bar graphs (**c**, **e-h**), violin plots (**j**) and overall transcript signatures of individual animals (**k**), or 95% confidence interval of linear regression (dashed lines) in correlation plot (**k**). Solid lines in violin plots (**j**) represent median, dotted lines represent 25th/75th percentiles, truncated at min-max values. *P* values indicate significant differences between groups (**c**, **d**), significance of correlation (**k**), or significant difference between SOD1^{G37R} mice treated with or without Cu^{II}(atsm) (shaded area, **b**; **e-h**, **j**)

Alox12 were least correlated with other genes (Supplementary Fig. 14a), and had the least impact on separating groups, despite PC2 accounting for 36% of the variance for *Gpx4* (Supplementary Fig. 14d). For genes associated with neurotoxic glial activation, PC1 accounted for 48.6% of total variance and separated ALS model mice and RSL3-treated glial cells from controls moreso than human ALS cases (Fig. 8b). Most genes contributed proportionately to this, with the exception of *Tgm1* and *Fbln5*, which in PC2 were opposingly elevated in ALS model mice and RSL3-treated glial cells compared

to human ALS cases, respectively (Supplementary Fig. 14e-h).

Discussion

The current common perception of ferroptosis is that it is an autonomously initiated cell suicide event [59]. Ferroptosis inducers or inhibitors have been used to interrogate the role of ferroptosis in in vivo models of neural disease, including Huntington's disease, Parkinson's disease, ALS, ischemic stroke and intracerebral haemorrhage [45, 60–64]. These studies, however, provide little insight into the
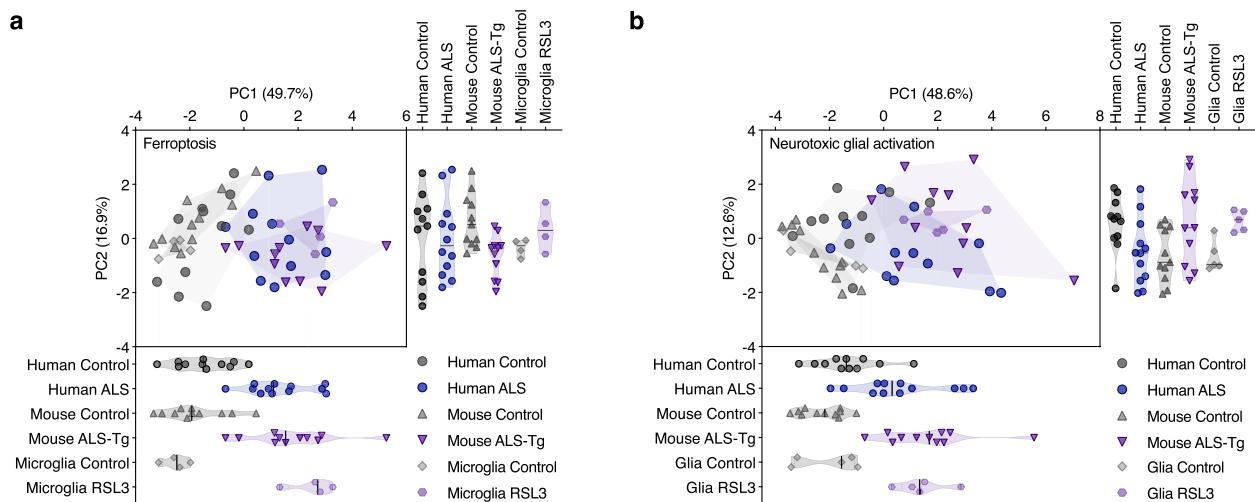
Liddell *et al. Molecular Neurodegeneration* (2024) 19:14

Page 16 of 21

Fig. 8 Principal component analysis of gene expression changes in human ALS-affected spinal cord compared to SOD1^{G37R} mice and cultured glia. Principal component analysis of genes associated with (**a**) ferroptosis and (**b**) neurotoxic glial activation in human ALS-affected spinal cord, SOD1^{G37R} mice, and glial cultures treated with the ferroptosis inducer RSL3. Individual values for PC1 and PC2 are projected below and to the right of the PCA plots, respectively. Symbols represent individual control and ALS cases, individual animals or independent glial cultures. Proportion of variance explained by each principal component is denoted on axes. Data are derived from z-scores of expression changes shown in Supplementary Figs. 3b, c, 7a, 9c, d and 12a

cellular consequences of ferroptosis and the results are generally interpreted as evidence for direct neuronal ferroptosis. Our findings necessitate a re-evaluation of these interpretations. Here we demonstrate a novel pathophysiological role for sublethal ferroptotic stress culminating in neuronal death in a non-cell autonomous manner. This proposition is supported by: results from primary glial and neuronal cells grown in culture (Figs. 2 and 3); its involvement in ALS being indicated by results from human ALS-affected spinal cord tissue (Figs. 1 and 4) and a robust animal model of the disease (Fig. 5); and therapeutic mitigation being evident in in vitro and in vivo experiments involving the CNS permeant ferroptosis inhibitor Cu^{II}(atsm) (Figs. 6 and 7).

As there are no specific markers of ferroptosis, its identification in tissue samples is established by the accumulation of consistent evidence across diverse markers. To date, different lines of evidence implicate ferroptosis in prominent neurodegenerative diseases including ALS. Here, our multifaceted analyses spanning atomic, molecular and biochemical indications provide the first comprehensive evidence indicating ferroptosis is a salient feature of sporadic ALS-affected spinal cord (Fig. 1). Moreover, these changes are recapitulated in a robust animal model of ALS (Fig. 5), supporting the veracity of this model to investigate ferroptosis in ALS.

Our findings indicate that ferroptotic stress preferentially influences microglia – the resident immune cells of the CNS – over other CNS cells. Firstly, we show microglia are more sensitive to overt ferroptosis than astrocytes

or neurones in vitro (Fig. 2), an observation in line with a recent study [65]. Secondly, we show sublethal ferroptotic stress causes lipid peroxidation, induction of ferroptosis-related genes and an inflammatory response in microglia, yet has no discernable impact on neurones or astrocytes. Of the ferroptosis-related genes induced by ferroptotic stress, many coding for lipoxygenases are specifically expressed by microglia (Fig. 2g). As lipoxygenases are involved in intitiation of ferroptosis [48], their specific expression by microglia in the CNS may contribute to the greater sensitivity of microglia to ferroptosis. In vivo evidence for microglial ferroptotic stress includes elevation of the microglial-specific lipoxygenases in sporadic ALS-affected tissue (Fig. 1) and ALS model mice (Fig. 5), and microglial-specific elevation of the widely expressed ferroptosis marker LPCAT3 in ALS model mice (Fig. 5k-n). Furthermore, we observe that the ferroptosis-related gene expression signatures are highly similar for ferroptosis-stimulated microglia in vitro, for sporadic ALS-affected tissue, and for ALS model mice (Supplementary Fig. 14). In line with this, microglial gene expression changes identified by RNAseq in response to ferroptotic stimuli are evident in human ALS-affected spinal cord [65]. Together, these data indicate that the emergence of ferroptotic stimuli in vivo, as evident in ALS, likely preferentially impact microglia.

Our findings demonstrate a novel pathophysiological role for sublethal microglial ferroptotic stress that culminates in neuronal death in a non-cell autonomous manner. When ferroptotic stress insufficient to induce cell death is

Liddell *et al. Molecular Neurodegeneration* (2024) 19:14

Page 17 of 21

applied to microglia, it triggers an inflammatory response that induces a neurotoxic glial phenotype that only occurs in the presence of astrocytes (Fig. 3). While microglia were recently reported to exacerbate ferroptosis-induced neuronal demise [65], our findings demonstrate initiation of this non-cell autonomous pathway to neuronal death can occur in the absence of overt ferroptotic cell death. Our results also illustrate the intercellular communication whereby microglia release factors that, while not directly toxic to neurones, induce a neurotoxic phenotype in astrocytes such that microglial ferroptotic stress results in neuronal death only in the presence of astrocytes. Furthermore, we find corroborative evidence for the presence of neurotoxic glia in sporadic ALS-affected tissue (Fig. 4) and the SOD1[G37R] mouse model of ALS (Fig. 5), where the gene expression signatures for neurotoxic glial activation are highly similar to ferroptosis-stimulated glia in vitro (Supplementary Fig. 14), and the expression signatures for ferroptosis genes and neurotoxic glia are correlated in both ALS-affected tissue (Fig. 4d) and ALS model mice (Fig. 7k). Thus, our results indicate that neuronal demise may not be the result of overt neuronal ferroptosis, but rather an inflammatory signalling pathway instigated by microglial ferroptotic stress in the absence of overt ferroptotic cell death. While precedent for this pathway has been demonstrated using the bacterial endotoxin LPS [16], our findings identify microglial ferroptotic stress as a disease-relevant trigger for this non-cell autonomous inflammatory signalling pathway to neuronal death.

The relevance of microglial activation of neurotoxic astrocytes in neurodegenerative disease was substantiated whereby genetic deletion of *Il1a*, *Tnf* and *C1qa* produced strong neuroprotective and disease-modifying outcomes in a SOD1[G93A] mouse model of ALS, including a 54% extension to survival [51]. Other disease-relevant triggers of neurotoxic glial activation include release of damaged mitochondria from microglia in cell culture models of ALS, Huntington's disease and Alzheimer's disease [66], and fibrils of α-synuclein in Parkinson's disease [67]. These studies support the assertion that inflammatory activation of microglia causes neurotoxic glial activation in neurodegeneration.

The role of ferroptosis in ALS is supported by the overexpression of GPX4 delaying symptom onset and improving survival of SOD1[G93A] ALS model mice [45, 46]. Our results lead us to propose that the ferroptotic stress-induced neurotoxic glia pathway is a treatable feature of ALS. In vitro, canonical ferroptosis inhibitors blocked upregulation of ferroptosis genes in microglia, prevented upregulation of neurotoxic glial activation genes and inhibited the neurotoxicity of ferroptosis-induced glial conditioned medium (Figs. 2 and 3). These results provide evidence for the causal relationship between ferroptosis

and neurotoxic glial activation. Furthermore, these effects were recapitulated by treatment with Cu[II](atsm) – a compound that we and others confirm has direct anti-ferroptotic activity (Fig. 6) [52, 53]. Cu[II](atsm) also suppressed markers of both ferroptosis and neurotoxic glia evident in the ALS model mice (Fig. 7). Other mechanisms have been proposed for the neuroprotective action of Cu[II](atsm), including delivery of copper, particularly to copper-deficient SOD1 [55], although these are not mutually exclusive with its potent anti-ferroptotic action. Together, these data demonstrate a causal relationship between microglial ferroptosis, neurotoxic astrocyte activation and neuronal death in vitro that is strongly corroborated in vivo.

GPX4 levels were recently reported as substantially [46] or mildly [45] diminished in ALS-afflicted spinal cord tissue. The former only compared ALS cases to 5 controls and provided no demographic data [46]. The latter was better powered, but the ALS cases were almost 20 years older than controls (49.8 ± 11.2 vs 68.6 ± 14.5, $p = 0.005$) [45], as compared to our study in which control and ALS cases were well matched (73.9 ± 12.9 vs 66.8 ± 8.9, $n = 11,15$, $P > 0.05$). Neither of these preceding studies report *GPX4* transcript, GPX4 activity or glutathione levels in human spinal cord. In contrast, both studies are concordant with our findings with respect to GPX4 protein and transcript levels in ALS model mice. At a minimum, this indicates potential case-to-case variability in GPX4 levels in human ALS spinal cord tissue, highlighting the need for sufficient case numbers. Regardless, an impaired glutathione-GPX4 system is a consistent finding across all these studies, in both ALS-afflicted spinal cord and ALS mouse models, which likely contributes to the emergence of ferroptotic stress.

Cu[II](atsm) has been extensively investigated in preclinical animal models of ALS, Parkinson's disease and stroke, invariably producing neuroprotective outcomes [68]. We have previously reported robust neuroprotective outcomes in multiple mutant SOD1 mouse models of ALS, including when Cu[II](atsm) is administered after symptom onset [28, 54–56]. These outcomes have been independently verified by multiple groups [58, 69, 70], including the first drug candidate to ever be validated by the ALS Therapy Development Institute [57]. On the strength of these findings, Cu[II](atsm) is under clinical development for the treatment of ALS and Parkinson's disease patients, completing early phase assessments [71, 72] with favourable results [73, 74] and has continued to phase II/III testing in ALS patients [75]. Histological assessment of a subset of ALS cases ($n = 6$) from these trials recently concluded that Cu[II](atsm) treatment had no significant pathological benefit [76], despite Cu[II](atsm) treatment associating with a > 80% decrease in neuronal TDP-43 pathology in motor cortex and

Liddell *et al. Molecular Neurodegeneration*   (2024) 19:14

Page 18 of 21

spinal cord ($p = 0.1$ and $p = 0.2$, respectively) and significantly diminishing microglial activation in spinal cord by 64% [77]. Thus, mitigation of microglial activation by the ferroptosis inhibitor Cu^{II}(atsm), associated with a trend towards diminished motor neuronal pathology in ALS patients, provides remarkable clinical validation of our findings.

Conclusions

Results presented herein provide the first evidence for reactive microglia responding to ferroptotic stress causing non-cell autonomous neuronal death. The neuropathology of diverse neurodegenerative conditions features reactive gliosis [78]. These diseases also exhibit signs of ferroptosis (including iron accumulation, glutathione depletion, and lipid peroxidation [79–82]) and the involvement of neurotoxic astrocytes is implicated [16]. Accordingly, the ferroptosis-neurotoxic glia pathway we describe here and illustrate in the context of ALS may contribute to neuronal death in other neurodegenerative diseases. By demonstrating that sublethal ferroptotic stress in microglia is a non-cell autonomous trigger of neuronal death, our discovery provides new understanding of how neurones die in neurodegenerative disease. These results also highlight that therapeutic strategies for neurodegenerative disease that target ferroptosis should not focus solely on neuronal events and need to address glial ferroptosis.

Abbreviations

ALOX5	Arachidonate 5-lipoxygenase
ALS	Amyotrophic lateral sclerosis
BSO	Buthionine sulphoximine
CNS	Central nervous system
C3	Complement component 3
ChAT	Choline O-acetyltransferase
DAPI	4′,6-Diamidino-2-phenylindole
DFN	Deferiprone
DMEM	Dulbecco's modified Eagle's medium
FAC	Ferric ammonium citrate
FBS	Foetal bovine serum
Fer1	Ferrostatin-1
GPX4	Glutathione peroxidase 4
IBA1	Ionised calcium-binding adapter molecule 1
ICP-MS	Inductively coupled plasma-mass spectrometry
IMDM	Iscove modified Dulbecco media
LDH	Lactate dehydrogenase
Lip1	Liproxstatin-1
LPCAT3	Lysophosphatidylcholine acyltransferase 3
LPS	Lipopolysaccharide
MTT	3-(4,5-Dimethylthiazol-2-yl)-2,5-diphenyltetrazolium bromide
PC-OOH	Phosphatidylcholine hydroperoxide
RCF	Relative centrifugal force
RSL3	(1S,3R)-Methyl-2-(2-chloroacetyl)-2,3,4,9-tetrahydro-1-[4-(methoxycarbonyl)phenyl]-1H-pyrido[3,4-b]indole-3-carboxylic acid
RT-PCR	Reverse transcription polymerase chain reaction
SDS-PAGE	Sodium dodecyl sulphate–polyacrylamide gel electrophoresis
SOD1	Superoxide dismutase 1
SSV	Standard suspension vehicle
TBS	Tris-buffered saline

Supplementary Information

The online version contains supplementary material available at https://doi.org/10.1186/s13024-023-00691-8.

Additional file 1: Supplementary Table 1. Case information of ALS-affected spinal cord samples. **Supplementary Figure 1.** Immunoblots for proteins examined in human and mouse spinal cord. **Supplementary Figure 2.** Iron content of human, ALS-affected spinal cord. **Supplementary Figure 3.** Gene expression changes in human, ALS-affected spinal cord. **Supplementary Figure 4.** GPX4 in spinal cord of human ALS cases and *Gpx4*(-/-) mice. **Supplementary Figure 5.** Microglial ferroptosis. **Supplementary Figure 6.** Retention of neurotoxic factor(s) by 30 kDa MWCO filter. **Supplementary Figure 7.** Gene expression changes used to monitor neurotoxic glial activation in response to ferroptotic stress in glial cells. **Supplementary Figure 8.** Isolating astrocytes from mixed glial cultures and gene expression changes in response to treatment with RSL3 or RSL3 plus iron. **Supplementary Figure 9.** Glutathione and gene expression changes in spinal cord of SOD1^{G37R} mice compared to non-transgenic littermates. **Supplementary Figure 10.** Changes in cellular expression of LPCAT3 in SOD1^{G37R} and *Gpx4*(-/-) mice. **Supplementary Figure 11.** Protective activity of Cu^{II}(atsm) *in vitro*. **Supplementary Figure 12.** Gene expression changes in glial cultures treated with inducers of ferroptosis and the metallocomplex Cu^{II}(atsm). **Supplementary Figure 13.** Effect of Cu^{II}(atsm) on glutathione and gene expression changes in SOD1^{G37R} mice. **Supplementary Figure 14.** Analysis of PCA for gene expression changes in human ALS-affected spinal cord compared to SOD1^{G37R} mice and RSL3-treated glial cultures.

Additional file 2: Supplementary Video 1. Live cell imaging of lipid peroxidation in mixed glial cultures treated with the ferroptosis inducer RSL3.

Additional file 3: Supplementary Video 2. Live cell imaging of lipid peroxidation in mixed glial cultures treated with various ferroptotic stimuli (RSL3, erastin+iron, and iron).

Additional file 4: Supplementary Video 3. Live cell imaging of lipid peroxidation in mixed glial cultures treated with BSO.

Additional file 5: Supplementary Video 4. Live cell imaging of showing mitigation of lipid peroxidation by the ferroptosis inhibitors, liproxstatin-1 (Lip1), Cu^{II}(atsm) and deferiprone (DFN) in isolated microglia treated with RSL3.

Additional file 6: Supplementary Video 5. Live cell imaging of showing mitigation of lipid peroxidation by the ferroptosis inhibitor Cu^{II}(atsm) in mixed glial cultures treated with RSL3.

Authors' contributions

JRL, JBWH, KK, AIB and PJC contributed to conception and design of the study, acquisition and analysis of data, and drafting the manuscript. JLB, SN, LEM, DJH, BP, SWM, AAB, SA, BRR, JSB, CAM, ARW and PSD contributed to acquisition and analysis of data.

Liddell *et al. Molecular Neurodegeneration* (2024) 19:14

Page 19 of 21

Availability of data and materials
The datasets used and/or analysed during the current study are available from the corresponding author on reasonable request.

Declarations

Ethics approval and consent to participate
The use of mice for generating primary cell cultures and assessing the effect of Cu^{II}(atsm) was approved by a University of Melbourne Animal Experimentation Committee (Projects 1613931, 1814576, and 1915081) and complied with National Health and Medical Research Council guidelines. Procedures involving post-mortem human tissue were approved by a University of Melbourne Human Ethics Committee (Projects ID 1238124 and 1750665).

Consent for publication
Not applicable.

Competing interests
Collaborative Medicinal Development LLC has licensed intellectual property related to this subject from the University of Melbourne where the inventors include ARW and PSD. AIB is a shareholder in Alterity Ltd, Cogstate Ltd, Brighton Biotech LLC, Grunbiotics Pty Ltd, Eucalyptus Pty Ltd, and Mesoblast Ltd. He is a paid consultant for Collaborative Medicinal Development LLC and has a profit share interest in Collaborative Medicinal Development Pty Ltd. PJC and JSB are unpaid consultants for Collaborative Medicinal Development LLC.

Author details
^{1}Department of Anatomy and Physiology, The University of Melbourne, Parkville, VIC 3010, Australia. ^{2}School of Chemistry and Bio21 Molecular Science and Biotechnology Institute, The University of Melbourne, Parkville, VIC 3010, Australia. ^{3}Atomic Medicine Initiative, University of Technology Sydney, Ultimo, NSW 2007, Australia. ^{4}School of Earth Science, The University of Melbourne, Parkville, VIC 3010, Australia. ^{5}Florey Institute of Neuroscience and Mental Health, The University of Melbourne, Parkville, VIC 3010, Australia. ^{6}Department of Biochemistry, Emory University, Atlanta, GA 30322, USA. ^{7}Linus Pauling Institute, Oregon State University, Corvallis, OR 97331, USA. ^{8}Anatomical Pathology, Alfred Hospital, Melbourne, VIC 3005, Australia. ^{9}QIMR Berghofer Medical Research Institute, Herston, QLD 4006, Australia.

References
1. Khakh BS, Deneen B. The emerging nature of astrocyte diversity. Annu Rev Neurosci. 2019;42:187–207.
2. Vainchtein ID, Molofsky AV. Astrocytes and microglia: in sickness and in health. Trends Neurosci. 2020;43(3):144–54.
3. Salter MW, Stevens B. Microglia emerge as central players in brain disease. Nat Med. 2017;23(9):1018–27.
4. Phatnani H, Maniatis T. Astrocytes in neurodegenerative disease. Cold Spring Harb Perspect Biol. 2015;7(6):a020628.
5. Kiernan MC, Vucic S, Cheah BC, Turner MR, Eisen A, Hardiman O, et al. Amyotrophic lateral sclerosis. Lancet. 2011;377(9769):942–55.
6. Di Giorgio FP, Boulting GL, Bobrowicz S, Eggan KC. Human embryonic stem cell-derived motor neurons are sensitive to the toxic effect of glial cells carrying an ALS-causing mutation. Cell Stem Cell. 2008;3(6):637–48.
7. Di Giorgio FP, Carrasco MA, Siao MC, Maniatis T, Eggan K. Non-cell autonomous effect of glia on motor neurons in an embryonic stem cell-based ALS model. Nat Neurosci. 2007;10(5):608–14.
8. Nagai M, Re DB, Nagata T, Chalazonitis A, Jessell TM, Wichterle H, et al. Astrocytes expressing ALS-linked mutated SOD1 release factors selectively toxic to motor neurons. Nat Neurosci. 2007;10(5):615–22.
9. Papadeas ST, Kraig SE, O'Banion C, Lepore AC, Maragakis NJ. Astrocytes carrying the superoxide dismutase 1 (SOD1G93A) mutation induce wild-type motor neuron degeneration in vivo. Proc Natl Acad Sci U S A. 2011;108(43):17803–8.
10. Qian K, Huang H, Peterson A, Hu B, Maragakis NJ, Ming GL, et al. Sporadic ALS astrocytes induce neuronal degeneration in vivo. Stem Cell Rep. 2017;8(4):843–55.
11. Boillee S, Yamanaka K, Lobsiger CS, Copeland NG, Jenkins NA, Kassiotis G, et al. Onset and progression in inherited ALS determined by motor neurons and microglia. Science. 2006;312(5778):1389–92.
12. Beers DR, Henkel JS, Xiao Q, Zhao W, Wang J, Yen AA, et al. Wild-type microglia extend survival in PU.1 knockout mice with familial amyotrophic lateral sclerosis. Proc Natl Acad Sci U S A. 2006;103(43):16021–6.
13. Wang L, Sharma K, Grisotti G, Roos RP. The effect of mutant SOD1 dismutase activity on non-cell autonomous degeneration in familial amyotrophic lateral sclerosis. Neurobiol Dis. 2009;35(2):234–40.
14. Yamanaka K, Chun SJ, Boillee S, Fujimori-Tonou N, Yamashita H, Gutmann DH, et al. Astrocytes as determinants of disease progression in inherited amyotrophic lateral sclerosis. Nat Neurosci. 2008;11(3):251–3.
15. Wang L, Gutmann DH, Roos RP. Astrocyte loss of mutant SOD1 delays ALS disease onset and progression in G85R transgenic mice. Hum Mol Genet. 2011;20(2):286–93.
16. Liddelow SA, Guttenplan KA, Clarke LE, Bennett FC, Bohlen CJ, Schirmer L, et al. Neurotoxic reactive astrocytes are induced by activated microglia. Nature. 2017;541(7638):481–7.
17. Masvekar R, Wu T, Kosa P, Barbour C, Fossati V, Bielekova B. Cerebrospinal fluid biomarkers link toxic astrogliosis and microglial activation to multiple sclerosis severity. Mult Scler Relat Disord. 2019;28:34–43.
18. Balu DT, Pantazopoulos H, Huang CCY, Muszynski K, Harvey TL, Uno Y, et al. Neurotoxic astrocytes express the d-serine synthesizing enzyme, serine racemase, in Alzheimer's disease. Neurobiol Dis. 2019;130:104511.
19. Dixon SJ, Lemberg KM, Lamprecht MR, Skouta R, Zaitsev EM, Gleason CE, et al. Ferroptosis: an iron-dependent form of nonapoptotic cell death. Cell. 2012;149(5):1060–72.
20. Riegman M, Sagie L, Galed C, Levin T, Steinberg N, Dixon SJ, et al. Ferroptosis occurs through an osmotic mechanism and propagates independently of cell rupture. Nat Cell Biol. 2020;22(9):1042–8.
21. Magtanong L, Dixon SJ. Ferroptosis and brain injury. Dev Neurosci. 2018;40(5–6):382–95.
22. Stockwell BR, Friedmann Angeli JP, Bayir H, Bush AI, Conrad M, Dixon SJ, et al. Ferroptosis: a regulated cell death nexus linking metabolism, redox biology, and disease. Cell. 2017;171(2):273–85.
23. Hamprecht B, Löffler F. Primary glial cultures as a model for studying hormone action. Methods Enzymol. 1985;109:341–5.
24. Choo XY, Liddell JR, Huuskonen MT, Grubman A, Moujalled D, Roberts J, et al. Cu^{II}(atsm) attenuates neuroinflammation. Front Neurosci. 2018;12:668.
25. Saura J, Tusell JM, Serratosa J. High-yield isolation of murine microglia by mild trypsinization. Glia. 2003;44(3):183–9.
26. Moujalled D, James JL, Yang S, Zhang K, Duncan C, Moujalled DM, et al. Phosphorylation of hnRNP K by cyclin-dependent kinase 2 controls cytosolic accumulation of TDP-43. Hum Mol Genet. 2015;24(6):1655–69.
27. Wong PC, Pardo CA, Borchelt DR, Lee MK, Copeland NG, Jenkins NA, et al. An adverse property of a familial ALS-linked SOD1 mutation causes motor neuron disease characterized by vacuolar degeneration of mitochondria. Neuron. 1995;14(6):1105–16.

Liddell *et al. Molecular Neurodegeneration* (2024) 19:14

Page 20 of 21

28. Hilton JB, Mercer SW, Lim NKH, Faux NG, Buncic G, Beckman JS, et al. Cu^{II}(atsm) improves the neurological phenotype and survival of SOD1^{G93A} mice and selectively increases enzymatically active SOD1 in the spinal cord. Sci Rep. 2017;7:42292.

29. Chen L, Hambright WS, Na R, Ran Q. Ablation of the ferroptosis inhibitor glutathione peroxidase 4 in neurons results in rapid motor neuron degeneration and paralysis. J Biol Chem. 2015;290(47):28097–106.

30. Hilton JB, Kysenius K, White AR, Crouch PJ. The accumulation of enzymatically inactive cuproenzymes is a CNS-specific phenomenon of the SOD1(G37R) mouse model of ALS and can be restored by overexpressing the human copper transporter hCTR1. Exp Neurol. 2018;307:118–28.

31. Hare DJ, Kysenius K, Paul B, Knauer B, Hutchinson RW, O'Connor C, et al. Imaging metals in brain tissue by laser ablation - inductively coupled plasma - mass spectrometry (LA-ICP-MS). J Vis Exp. 2017. https://doi.org/10.3791/55042(119).

32. Kysenius K, Paul B, Hilton JB, Liddell JR, Hare DJ, Crouch PJ. A versatile quantitative microdroplet elemental imaging method optimised for integration in biochemical workflows for low-volume samples. Anal Bioanal Chem. 2019;411(3):603–16.

33. Wong BX, Ayton S, Lam LQ, Lei P, Adlard PA, Bush AI, et al. A comparison of ceruloplasmin to biological polyanions in promoting the oxidation of Fe(2+) under physiologically relevant conditions. Biochim Biophys Acta. 2014;1840(12):3299–310.

34. Liddell JR, Lehtonen S, Duncan C, Keksa-Goldsteine V, Levonen AL, Goldsteins G, et al. Pyrrolidine dithiocarbamate activates the Nrf2 pathway in astrocytes. J Neuroinflammation. 2016;13:49.

35. Roveri A, Flohe L, Maiorino M, Ursini F. Phospholipid-hydroperoxide glutathione peroxidase in sperm. Methods Enzymol. 2002;347:208–12.

36. Maiorino M, Gregolin C, Ursini F. Phospholipid hydroperoxide glutathione peroxidase. Methods Enzymol. 1990;186:448–57.

37. Motulsky HJ, Brown RE. Detecting outliers when fitting data with nonlinear regression - a new method based on robust nonlinear regression and the false discovery rate. BMC Bioinformatics. 2006;7:123.

38. Kwan JY, Jeong SY, Van Gelderen P, Deng HX, Quezado MM, Danielian LE, et al. Iron accumulation in deep cortical layers accounts for MRI signal abnormalities in ALS: correlating 7 tesla MRI and pathology. PLoS One. 2012;7(4):e35241.

39. Adachi Y, Sato N, Saito Y, Kimura Y, Nakata Y, Ito K, et al. Usefulness of SWI for the detection of iron in the motor cortex in amyotrophic lateral sclerosis. J Neuroimaging. 2015;25(3):443–51.

40. Ignjatovic A, Stevic Z, Lavrnic S, Dakovic M, Bacic G. Brain iron MRI: a biomarker for amyotrophic lateral sclerosis. J Magn Reson Imaging. 2013;38(6):1472–9.

41. Ince PG, Shaw PJ, Candy JM, Mantle D, Tandon L, Ehmann WD, et al. Iron, selenium and glutathione peroxidase activity are elevated in sporadic motor neuron disease. Neurosci Lett. 1994;182(1):87–90.

42. Ayton S, Lei P, Duce JA, Wong BX, Sedjahtera A, Adlard PA, et al. Ceruloplasmin dysfunction and therapeutic potential for Parkinson disease. Ann Neurol. 2013;73(4):554–9.

43. Jeong SY, David S. Glycosylphosphatidylinositol-anchored ceruloplasmin is required for iron efflux from cells in the central nervous system. J Biol Chem. 2003;278(29):27144–8.

44. Yang WS, SriRamaratnam R, Welsch ME, Shimada K, Skouta R, Viswanathan VS, et al. Regulation of ferroptotic cancer cell death by GPX4. Cell. 2014;156(1–2):317–31.

45. Chen L, Na R, Danae McLane K, Thompson CS, Gao J, Wang X, et al. Over-expression of ferroptosis defense enzyme Gpx4 retards motor neuron disease of SOD1G93A mice. Sci Rep. 2021;11(1):12890.

46. Wang T, Tomas D, Perera ND, Cuic B, Luikinga S, Viden A, et al. Ferroptosis mediates selective motor neuron death in amyotrophic lateral sclerosis. Cell Death Differ. 2022;29(6):1187–98.

47. Trist BG, Genoud S, Roudeau S, Rookyard A, Abdeen A, Cottam V, et al. Altered SOD1 maturation and post-translational modification in amyotrophic lateral sclerosis spinal cord. Brain. 2022;145(9):3108–30.

48. Shah R, Shchepinov MS, Pratt DA. Resolving the role of lipoxygenases in the initiation and execution of ferroptosis. ACS Cent Sci. 2018;4(3):387–96.

49. Drummen GP, van Liebergen LC, Op den Kamp JA, Post JA. C11-BODIPY(581/591), an oxidation-sensitive fluorescent lipid peroxidation probe: (micro)spectroscopic characterization and validation of methodology. Free Radic Biol Med. 2002;33(4):473–90.

50. Zhang Y, Sloan SA, Clarke LE, Caneda C, Plaza CA, Blumenthal PD, et al. Purification and characterization of progenitor and mature human astrocytes reveals transcriptional and functional differences with mouse. Neuron. 2016;89(1):37–53.

51. Guttenplan KA, Weigel MK, Adler DI, Couthouis J, Liddelow SA, Gitler AD, et al. Knockout of reactive astrocyte activating factors slows disease progression in an ALS mouse model. Nat Commun. 2020;11(1):3753.

52. Southon A, Szostak K, Acevedo KM, Dent KA, Volitakis I, Belaidi AA, et al. Cu^{II}(atsm) inhibits ferroptosis: implications for treatment of neurodegenerative disease. Br J Pharmacol. 2020;177(3):656–67.

53. Zilka O, Poon J-F, Pratt DA. Radical-trapping antioxidant activity of copper and nickel bis(thiosemicarbazone) complexes underlies their potency as inhibitors of ferroptotic cell death. J Am Chem Soc. 2021;143(45):19043–57.

54. McAllum EJ, Lim NKH, Hickey JL, Paterson BM, Donnelly PS, Li QX, et al. Therapeutic effects of Cu^{II}(atsm) in the SOD1G37R mouse model of amyotrophic lateral sclerosis. Amyotroph Lateral Scler Frontotemporal Degener. 2013;14(7–8):586–90.

55. Roberts BR, Lim NK, McAllum EJ, Donnelly PS, Hare DJ, Doble PA, et al. Oral treatment with Cu^{II}(atsm) increases mutant SOD1 in vivo but protects motor neurons and improves the phenotype of a transgenic mouse model of amyotrophic lateral sclerosis. J Neurosci. 2014;34(23):8021–31.

56. Soon CP, Donnelly PS, Turner BJ, Hung LW, Crouch PJ, Sherratt NA, et al. Diacetylbis(N(4)-methylthiosemicarbazonato) copper(II) (CuII(atsm)) protects against peroxynitrite-induced nitrosative damage and prolongs survival in amyotrophic lateral sclerosis mouse model. J Biol Chem. 2011;286(51):44035–44.

57. Vieira FG, Hatzipetros T, Thompson K, Moreno AJ, Kidd JD, Tassinari VR, et al. CuATSM efficacy is independently replicated in a SOD1 mouse model of ALS while unmetallated ATSM therapy fails to reveal benefits. IBRO Rep. 2017;2:47–53.

58. Williams JR, Trias E, Beilby PR, Lopez NI, Labut EM, Bradford CS, et al. Copper delivery to the CNS by CuATSM effectively treats motor neuron disease in SOD mice co-expressing the Copper-Chaperone-for-SOD. Neurobiol Dis. 2016;89:1–9.

59. Han C, Liu Y, Dai R, Ismail N, Su W, Li B. Ferroptosis and its potential role in human diseases. Front Pharmacol. 2020;11:239.

60. Van Do B, Gouel F, Jonneaux A, Timmerman K, Gele P, Petrault M, et al. Ferroptosis, a newly characterized form of cell death in Parkinson's disease that is regulated by PKC. Neurobiol Dis. 2016;94:169–78.

61. Li Q, Han X, Lan X, Gao Y, Wan J, Durham F, et al. Inhibition of neuronal ferroptosis protects hemorrhagic brain. JCI Insight. 2017;2(7):e90777.

62. Skouta R, Dixon SJ, Wang J, Dunn DE, Orman M, Shimada K, et al. Ferrostatins inhibit oxidative lipid damage and cell death in diverse disease models. J Am Chem Soc. 2014;136(12):4551–6.

63. Moreau C, Danel V, Devedjian JC, Grolez G, Timmerman K, Laloux C, et al. Could conservative iron chelation lead to neuroprotection in amyotrophic lateral sclerosis? Antioxid Redox Signal. 2018;29(8):742–8.

64. Tuo QZ, Lei P, Jackman KA, Li XL, Xiong H, Li XL, et al. Tau-mediated iron export prevents ferroptotic damage after ischemic stroke. Mol Psychiatry. 2017;22(11):1520–30.

65. Ryan SK, Zelic M, Han Y, Teeple E, Chen L, Sadeghi M, et al. Microglia ferroptosis is regulated by SEC24B and contributes to neurodegeneration. Nat Neurosci. 2023;26(1):12–26.

66. Joshi AU, Minhas PS, Liddelow SA, Haileselassie B, Andreasson KI, Dorn GW 2nd, et al. Fragmented mitochondria released from microglia trigger A1 astrocytic response and propagate inflammatory neurodegeneration. Nat Neurosci. 2019;22(10):1635–48.

67. Yun SP, Kam TI, Panicker N, Kim S, Oh Y, Park JS, et al. Block of A1 astrocyte conversion by microglia is neuroprotective in models of Parkinson's disease. Nat Med. 2018;24(7):931–8.

68. Nikseresht S, Hilton JBW, Kysenius K, Liddell JR, Crouch PJ. Copper-ATSM as a treatment for ALS: support from mutant SOD1 models and beyond. Life. 2020;10(11):271.

69. Kuo MTH, Beckman JS, Shaw CA. Neuroprotective effect of CuATSM on neurotoxin-induced motor neuron loss in an ALS mouse model. Neurobiol Dis. 2019;130:104495.

70. Lum JS, Brown ML, Farrawell NE, McAlary L, Ly D, Chisholm CG, et al. CuATSM improves motor function and extends survival but is not

Liddell *et al. Molecular Neurodegeneration* (2024) 19:14

Page 21 of 21

tolerated at a high dose in SOD1(G93A) mice with a C57BL/6 background. Sci Rep. 2021;11(1):19392.

71. NCT02870634. ClinicalTrials.gov study # NCT02870634 "Phase 1 dose escalation and PK study of Cu(II)ATSM in ALS/MND".

72. NCT03204929. ClinicalTrials.gov study # NCT03204929 "Dose escalation study of Cu(II)ATSM in Parkinson's disease".

73. Rowe D, Mathers S, Smith G, Windebank E, Rogers M-L, Noel K, et al. Modification of ALS disease progression in a phase 1 trial of CuATSM. Amyotroph Lateral Scler Frontotemporal Degener. 2018;19(Suppl 1):264–81.

74. Rowe D, Mathers S, Noel K, Rosenfeld C. CuATSM phase 2a study confirms disease-modifying effects in patients with sporadic ALS observed in the phase 1 study (1338). Neurology. 2020;94(15 Supplement):1338.

75. NCT04082832. ClinicalTrials.gov study # NCT04082832 "CuATSM compared with placebo for treatment of ALS/MND".

76. Yang Y, Rowe D, McCann H, Shepherd CE, Kril JJ, Kiernan MC, et al. Treatment with the copper compound CuATSM has no significant effect on motor neuronal pathology in patients with ALS. Neuropathol Appl Neurobiol. 2023;49(4):e12919.

77. Liddell JR, Hilton JBW, Crouch PJ. CuII(atsm) significantly decreases microglial reactivity in patients with sporadic ALS. Neuropathol Appl Neurobiol. 2023;49(5):e12938.

78. Amor S, Peferoen LA, Vogel DY, Breur M, van der Valk P, Baker D, et al. Inflammation in neurodegenerative diseases–an update. Immunology. 2014;142(2):151–66.

79. Ghassaban K, Liu S, Jiang C, Haacke EM. Quantifying iron content in magnetic resonance imaging. Neuroimage. 2019;187:77–92.

80. Lee JH, Yun JY, Gregory A, Hogarth P, Hayflick SJ. Brain MRI pattern recognition in neurodegeneration with brain iron accumulation. Front Neurol. 2020;11:1024.

81. Aoyama K, Nakaki T. Impaired glutathione synthesis in neurodegeneration. Int J Mol Sci. 2013;14(10):21021–44.

82. Reed TT. Lipid peroxidation and neurodegenerative disease. Free Radic Biol Med. 2011;51(7):1302–19.

Publisher's Note

Springer Nature remains neutral with regard to jurisdictional claims in published maps and institutional affiliations.